Impacts of Internal Curing on the Performance of Concrete Materials in the Laboratory and the Field

Final Report
November 2017

National Concrete Pavement Technology Center

Tech Center

IOWA STATE UNIVERSITY
Institute for Transportation

Sponsored by
Iowa Highway Research Board
(Part of IHRB Project TR-676)
Iowa Department of Transportation
(Part of InTrans Project 14-499)

About the National CP Tech Center

The mission of the National Concrete Pavement Technology Center is to unite key transportation stakeholders around the central goal of advancing concrete pavement technology through research, tech transfer, and technology implementation.

Disclaimer Notice

The contents of this report reflect the views of the authors, who are responsible for the facts and the accuracy of the information presented herein. The opinions, findings and conclusions expressed in this publication are those of the authors and not necessarily those of the sponsors.

The sponsors assume no liability for the contents or use of the information contained in this document. This report does not constitute a standard, specification, or regulation.

The sponsors do not endorse products or manufacturers. Trademarks or manufacturers' names appear in this report only because they are considered essential to the objective of the document.

Iowa State University Non-Discrimination Statement

Iowa State University does not discriminate on the basis of race, color, age, ethnicity, religion, national origin, pregnancy, sexual orientation, gender identity, genetic information, sex, marital status, disability, or status as a U.S. veteran. Inquiries regarding non-discrimination policies may be directed to Office of Equal Opportunity, 3410 Beardshear Hall, 515 Morrill Road, Ames, Iowa 50011, Tel. 515–294–7612, Hotline: 515–294–1222, email eooffice@iastate.edu.

Iowa Department of Transportation Statements

Federal and state laws prohibit employment and/or public accommodation discrimination on the basis of age, color, creed, disability, gender identity, national origin, pregnancy, race, religion, sex, sexual orientation or veteran's status. If you believe you have been discriminated against, please contact the Iowa Civil Rights Commission at 800-457-4416 or the Iowa Department of Transportation affirmative action officer. If you need accommodations because of a disability to access the Iowa Department of Transportation's services, contact the agency's affirmative action officer at 800-262-0003.

The preparation of this report was financed in part through funds provided by the Iowa Department of Transportation through its "Second Revised Agreement for the Management of Research Conducted by Iowa State University for the Iowa Department of Transportation" and its amendments.

The opinions, findings, and conclusions expressed in this publication are those of the authors and not necessarily those of the Iowa Department of Transportation.

Technical Report Documentation Page

1. Report No.	2. Government Accession No.	3. Recipient's Catalog No.
Part of IHRB Project TR-676		

4. Title and Subtitle	5. Report Date
Impacts of Internal Curing on the Performance of Concrete Materials in the Laboratory and the Field	November 2017
	6. Performing Organization Code

7. Author(s)	8. Performing Organization Report No.
Payam Vosoughi (orcid.org/0000-0003-4317-0424), Peter Taylor (orcid.org/0000-0002-4030-1727), and Halil Ceylan (orcid.org/0000-0003-1133-0366)	Part of InTrans Project 14-499

9. Performing Organization Name and Address	10. Work Unit No. (TRAIS)
National Concrete Pavement Technology Center Iowa State University 2711 South Loop Drive, Suite 4700 Ames, IA 50010-8664	**11. Contract or Grant No.**

12. Sponsoring Organization Name and Address	13. Type of Report and Period Covered
Iowa Highway Research Board Iowa Department of Transportation 800 Lincoln Way Ames, IA 50010	Final Report
	14. Sponsoring Agency Code Part of IHRB Project TR-676

15. Supplementary Notes

Visit www.intrans.iastate.edu and www.cptechcenter.org for color pdfs of this and other research reports.

16. Abstract

Internal curing is a technique to prolong cement hydration by providing internal water reservoirs in a concrete mixture. These reservoirs do not affect the initial water-to-cementitious materials (w/cm) ratio, but do provide water for curing throughout the thickness of the element.

Benefits of this approach include improved mechanical properties as well as reduced risk of moisture gradients, thus reducing the potential for warping.

The aim of this work was to assess whether joint spacings could be increased in slabs containing lightweight fine aggregate (LWFA) as a source of internal curing.

17. Key Words	18. Distribution Statement
concrete mix design—concrete pavement performance—conventionally cured concrete—internally cured concrete—jointed concrete pavement—lightweight fine aggregate	No restrictions.

19. Security Classification (of this report)	20. Security Classification (of this page)	21. No. of Pages	22. Price
Unclassified.	Unclassified.	56	NA

Form DOT F 1700.7 (8-72) **Reproduction of completed page authorized**

IMPACTS OF INTERNAL CURING ON THE PERFORMANCE OF CONCRETE MATERIALS IN THE LABORATORY AND THE FIELD

Final Report
November2017

Principal Investigator
Peter Taylor, Director
National Concrete Pavement Technology Center, Iowa State University

Co-Principal Investigator
Halil Ceylan, Director
Program for Sustainable Pavement Engineering and Research (ProSPER)
Institute for Transportation, Iowa State University

Research Assistant
Payam Vosoughi

Authors
Payam Vosoughi, Peter Taylor, Halil Ceylan

Sponsored by
Iowa Highway Research Board and
Iowa Department of Transportation
(Part of IHRB Project TR-676)

Preparation of this report was financed in part
through funds provided by the Iowa Department of Transportation
through its Research Management Agreement with the
Institute for Transportation
(Part of InTrans Project 14-499)

A report from
National Concrete Pavement Technology Center
Iowa State University
2711 South Loop Drive, Suite 4700
Ames, IA 50010-8664
Phone: 515-294-5798 / Fax: 515-294-0467
www.intrans.iastate.edu

TABLE OF CONTENTS

ACKNOWLEDGMENTS ix
INTRODUCTION 1
WORK PLAN 2
MATERIAL PROPERTIES 2
MIXTURE PROPORTIONS 4
SITE LOCATION 5
EXPERIMENTAL METHODS 8
Moisture Content 10
Pore Water Pressure in Fresh Concrete 12
Portable Device for Measuring Curling and Warping of Concrete Pavements 14
RESULTS AND DISCUSSION 16
Early-Age Properties 16
Hardened Properties 22
CONCLUSIONS 34
REFERENCES 35
APPENDIX A: CYCLIC WETTING AND DRYING REGIME 37
APPENDIX B: MONITORING JOINT CRACKING OF CONTROL AND IC SECTIONS 39

LIST OF FIGURES

Figure 1. Aggregate gradations 4
Figure 2. Site plan of the constructed sidewalk 6
Figure 3. Placing concrete and embedding sensors 7
Figure 4. Obtaining test specimens in the field 7
Figure 5. Constructed sidewalk (IC section) 8
Figure 6. Calorimetry test device 9
Figure 7. Surface electrical resistivity test device (four-probe Wenner-Array device) 9
Figure 8. Preparation of a specimen for sorptivity testing 9
Figure 9. Measuring the CTE 10
Figure 10. Practical calibration equation for different soil materials 11
Figure 11. Decagon 5TE sensor for measuring relative dielectric permittivity, electrical resistivity, and temperature 11
Figure 12. Installation of Decagon 5TE sensors at the top and bottom layers of JPCP 12
Figure 13. Variation of water content and development of pore water pressure in early-age concrete mixtures 13
Figure 14. Capillary pressure sensor system 14
Figure 15. Upward (left) and downward (right) deformation of concrete pavement due to curling or warping 14
Figure 16. Portable device for measuring deflection over time 15
Figure 17. Digital height gauge used for measurements 15
Figure 18. Ten measurement points on two lines for monitoring curling and warping on a concrete slab 16
Figure 19. Semi-adiabatic calorimetry test results for laboratory mixtures 17
Figure 20. Variation in relative permittivity of laboratory mixtures at early ages 18
Figure 21. Variation in electrical conductivity of laboratory mixtures at early ages 18
Figure 22. Temperature variation in control concrete in the field 19
Figure 23. Relative permittivity variation in control concrete in the field 20
Figure 24. Temperature variation in IC concrete in the field 20
Figure 25. Relative permittivity variation in IC concrete in the field 21
Figure 26. PWP development in fresh concrete in laboratory mixtures 21
Figure 27. Surface electrical resistivity of laboratory specimens 23
Figure 28. Surface electrical resistivity of field specimens 23
Figure 29. Sorptivity test – control concrete 24
Figure 30. Sorptivity test – IC concrete 25
Figure 31. Customized calibration of VWC versus relative permittivity of control and IC concrete 26
Figure 32. Temperature variation over time between top and bottom layers 27
Figure 33. Variation in VWC between top and bottom layers 28
Figure 34. Built-in variation for control section, morning, 8 ft 28
Figure 35. Built-in variation for control section, morning, 12 ft 29
Figure 36. Built-in variation for IC section, morning, 8 ft 29
Figure 37. Built-in variation for IC section, morning, 12 ft 29
Figure 38. Built-in variation for control section, evening, 8 ft 30
Figure 39. Built-in variation for control section, evening, 12 ft 30

Figure 40. Built-in variation for IC section, evening, 8 ft 30
Figure 41. Built-in variation for IC section, evening, 12 ft 31
Figure 42. Curling and warping displacement at the north side of the control and IC concrete sections with 8 ft joint spacing 31
Figure 43. Curling and warping displacement at the south side of the control and IC concrete sections with 8 ft joint spacing 32
Figure 44. Curling and warping displacement at the north side of the control and IC concrete sections with 12 ft joint spacing 32
Figure 45. Curling and warping displacement at the south side of the control and IC concrete sections with 12 ft joint spacing 33
Figure 46. Summary of maximum vertical displacements 33
Figure 47. Cyclic wetting and drying regime at 50°C 37
Figure 48. Cyclic wetting and drying regime at 110°C 38
Figure 49. Schematic plan of joints in the control section.....39
Figure 50. Joint 1 in the control section.....39
Figure 51. Joint 2 in the control section.....39
Figure 52. Joint number 3 in the control section 40
Figure 53. Joint 4 in the control section.....40
Figure 54. Joint 5 in the control section.....40
Figure 55. Joint 6 in the control section.....41
Figure 56. Results of ultrasonic shear-wave tomography for cracked joints diagnostics.....42
Figure 57. Schematic plan of joints in the IC section 43
Figure 58. Joint 1 in the IC section 43
Figure 59. Joint 2 in the IC section 43
Figure 60. Joint 3 in the IC section 44
Figure 61. Joint 4 in the IC section 44
Figure 62. Joint 5 in the IC section 44
Figure 63. Joint 6 in the IC section 45
Figure 64. Joint 7 in the IC section 45
Figure 65. Joint 8 in the IC section 45
Figure 66. Joint 9 in the IC section 46
Figure 67. Joint 10 in the IC section 46

LIST OF TABLES

Table 1. Chemical compositions of portland cement (Type I/II) and fly ash (Class C) 3
Table 2. Cumulative percent passing gradation of aggregates 3
Table 3. Properties of LWFA used for internal curing 4
Table 4. Mixture proportion design of control and IC concrete 5
Table 5. Relative permittivity values of common materials in construction industry 11
Table 6. Fresh properties of concrete mixtures prepared in the laboratory 16
Table 7. Fresh properties of concrete mixtures sampled in the field 17
Table 8. Results of calorimetry test for laboratory mixtures 17
Table 9. Results of PWP development test in fresh concrete in laboratory mixtures 22
Table 10. Mechanical properties of laboratory mixtures 22
Table 11. Mechanical properties of field mixtures 22
Table 12. Water desorption, sorption, absorption, and rate of absorption of laboratory specimens 24
Table 13. Water desorption, sorption, and absorption of field specimens 25

ACKNOWLEDGMENTS

The research team would like to acknowledge the Iowa Highway Research Board and the Iowa Department of Transportation for sponsoring this research. They would also like to thank Larry Ford with Manatts, Inc., Daron Brown with Trinity Lightweight (Expanded Shale & Clay), and Bob Catus with Facilities Planning and Management at Iowa State University.

INTRODUCTION

Concrete curing involves techniques and methods to maintain the moisture and temperature of fresh concrete within desired ranges at early ages to ensure continued strength and durability development due to the hydration of cementitious materials. ACI committee 308 (ACI 308 2016) recommends 7-day and 10-day curing for concrete mixtures that incorporate Type I and II portland cement, respectively. However, concrete mixtures containing supplementary cementitious materials reportedly need to be cured for up to 14 days.

Depending on the application and design characteristics, a variety of curing regimes can be used, including external wet curing, insulation membrane curing, and internal curing.

Maintaining adequate moisture content is crucial for facilitating hydration reactions in portland cement concrete mixtures (Bentz and Snyder 1999). The aim of internal curing is to provide water reservoirs inside the body of concrete that aid curing throughout the section without affecting the water-to-cementituous materials (w/cm) ratio of the mixture. Internal curing thus provides cementitious material particles with enough moisture for the hydration reactions, but negative capillary pressures in the pores are reduced, leading to reduced shrinkage (Babcock and Taylor 2015, Bentz and Weiss 2011, Byard and Schindler 2010).

The beneficial effects of internal curing are especially apparent when it is used in mixtures with a water-to-cement ratio lower than 0.42 (De la Varga et al. 2014, Justs et al. 2015), where the risk of desiccation is high and external water cannot easily penetrate into the concrete.

The advantages of internally cured (IC) concrete over conventionally cured concrete are as follows:

- Improved hydration in terms of uniform moisture distribution through the mixture (Bentz and Snyder 1999)

- Reduced autogenous, plastic, and drying shrinkage, which leads to a lower likelihood of shrinkage cracking (Hartman et al. 2014, Shen et al. 2015, Wyrzykowski and Lura 2015)

- Reduced concrete permeability (De la Varga et al. 2014) and enhanced resistance to sulfate attack (Bentz et al. 2014)

- Improved strength and permeability at the interface transition zone (ITZ) (Bentz and Stutzman 2008, Sun et al. 2015)

- Reduced modulus of elasticity (MoE) and enhanced residual stress relaxation due to the presence of lightweight aggregates (LWAs) or superabsorbent polymers (SAPs) (Schlitter et al. 2013, Shen et al. 2016)

- Reduced moisture gradient along the concrete section, leading to reduced warping in concrete pavements (Kim et al. 2016)

- Reduced coefficient of thermal expansion (CTE) and thermal conductivity of concrete, resulting in reduced temperature gradients throughout the concrete section and reduced curling in concrete pavements (Amirkhanian and Roesler 2017, Byard et al. 2014)

LWAs and SAPs are two common materials used for internal curing. LWAs are cheaper and more available than SAPs in the United States and are therefore more widely employed.

The aim of this report is to investigate the effects of internal curing on the performance of practical concrete mixtures designed for the construction of jointed plain concrete pavements (JPCPs) in the state of Iowa. The study involved both laboratory investigation and field implementation and monitoring.

WORK PLAN

The research plan involved the construction of a sidewalk using a control mixture and a mixture containing lightweight fine aggregates (LWFAs). Samples of the mixtures were taken at the time of placement and sent to the laboratory for testing. Similar mixtures using the same materials were also prepared in the laboratory for comparison and additional testing. In addition, a number of sensors were embedded in the sidewalk concrete to monitor moisture and temperature over time. Periodic measurements were also taken throughout the winter to observe the dimensional stability of the slabs.

MATERIAL PROPERTIES

Type I/II portland cement (ASTM C150) and Class C fly ash (ASTM C618) were used for the preparation of both the control and LFWA mixtures. The chemical compositions of the cementitious materials are summarized in Table 1.

Table 1. Chemical compositions of portland cement (Type I/II) and fly ash (Class C)

Chemical composition	Type I/II cement	Class C fly ash
SiO_2	20.10	36.71
Al_2O_3	4.44	19.42
Fe_2O_3	3.09	6.03
SO_3	3.18	1.97
CaO	62.94	25.15
MgO	2.88	4.77
Na_2O	0.10	1.64
K_2O	0.61	0.46
P_2O_5	0.06	0.84
TiO_2	0.24	1.84
SrO	0.09	0.32
BaO	-	0.67
LOI	2.22	0.18

An air entraining agent complying with the specifications of ASTM C260 was incorporated into the mixtures. Some mixtures contained a commercially available water reducing admixture complying with ASTM C494.

Crushed limestone with a one-inch nominal maximum aggregate size (NMAS) was used as coarse aggregate, and river sand was used as fine aggregate. Table 2 summarizes the aggregate gradations.

Table 2. Cumulative percent passing gradation of aggregates

Sieve Size		Coarse aggregate	Fine aggregate
No.	mm		
1-1/2”	37	100.0	100.0
1”	25	99.3	100.0
3/4”	19	74.9	100.0
1/2”	12.5	37.0	100.0
3/8”	9.5	19.2	100.0
#4	4.75	2.7	98.9
#8	2.36	0.7	92.4
#16	1.18	0.5	77.5
#30	0.6	0.4	47.7
#50	0.3	0.4	11.0
#100	0.15	0.3	0.8
#200	0.075	0.3	0.0

The specific gravities of the coarse and fine aggregates were 2.68 and 2.66, respectively. The LWFA was a commercially available product. The properties and gradation of the LWFA employed for internal curing are indicated in Table 3 and Figure 1.

Table 3. Properties of LWFA used for internal curing

LWFA type	Specific gravity	Absorption (%)		Desorption at 93% relative humidity (%)
		24 hours	Ultimate	
Expanded clay	1.23	22.2	32.6	92

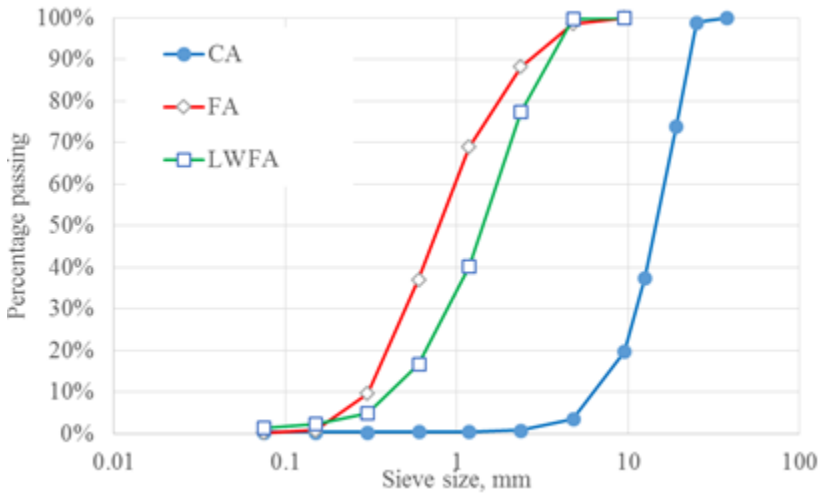

Figure 1. Aggregate gradations

MIXTURE PROPORTIONS

The mixture proportions of both the control and IC concrete used in both the field and laboratory studies are shown in Table 4. The proportions were based on those traditionally used for sidewalk construction. For the IC mixture, about 20% of the volume of fine aggregate was replaced by LWFA in order to provide 7% internal curing water by mass of cementitious materials (Schlitter et al. 2010).

Table 4. Mixture proportion design of control and IC concrete

	Control concrete	IC concrete
Portland cement (lb/yd^3)	457	457
Fly Ash (lb/yd^3)	114	114
Coarse aggregate (lb/yd^3)	1,698	1,698
Fine aggregate (lb/yd^3)	1375	942
Lightweight fine aggregate (lb/yd^3)	0	200
w/cm ratio	0.45	0.45
Fly ash percentage, by mass (%)	20	20
Target air content (%)	6	6

The concrete was prepared and delivered by a local ready-mix supplier. The LWFA was saturated prior to batching.

SITE LOCATION

The site plan of the constructed sidewalk on the Iowa State University campus is illustrated in Figure 2. Some slabs at the both ends of the control and IC sections have 8 ft joint spacing, while other slabs have 12 ft joint spacing.

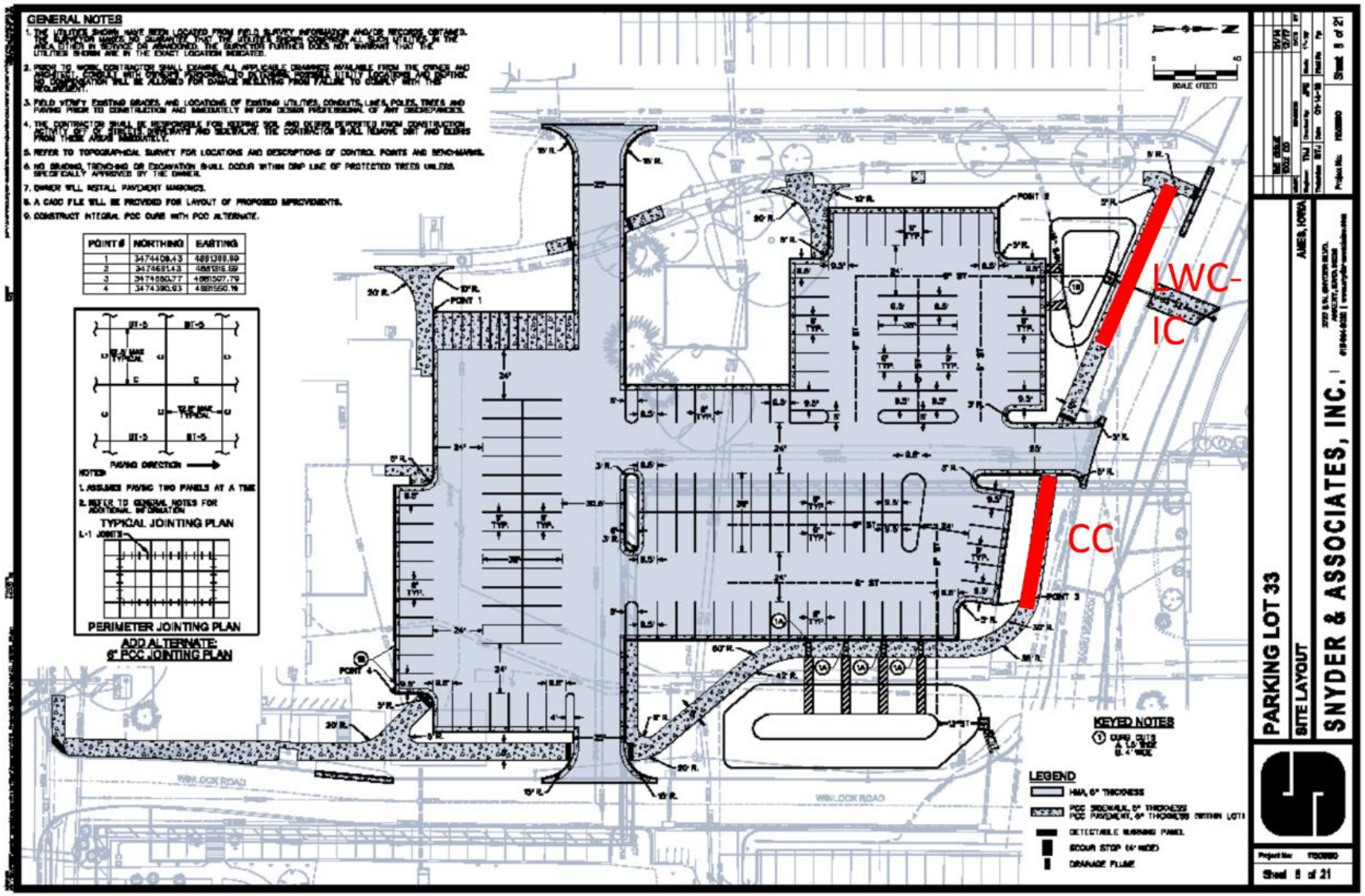

Figure 2. Site plan of the constructed sidewalk

Figures 3 and 4 show sensor installation and field sampling.

Figure 3. Placing concrete and embedding sensors

Figure 4. Obtaining test specimens in the field

The IC section of the constructed sidewalk is shown in Figure 5.

Figure 5. Constructed sidewalk (IC section)

EXPERIMENTAL METHODS

A wide range of standard laboratory and field tests were conducted:

- Workability of fresh concrete, slump test (ASTM C143)
- Air content of fresh concrete, pressure method (ASTM C231)
- Semi-adiabatic calorimetry (ASTM C1753) (see Figure 6)
- Compressive strength (ASTM C39)
- Static modulus of elasticity (MoE) (ASTM C469)
- Splitting tensile strength (ASTM C496)
- Electrical surface resistivity (AASHTO T 358) (see Figure 7)
- Rate of water absorption (ASTM C1585) (see Figure 8)
- Bulk water absorption of dried concrete specimen (ASTM C642)
- Bulk water sorption of dried concrete specimen (ASTM C1757)
- CTE of concrete (AASHTO T 336) (see Figure 9)

Figure 6. Calorimetry test device

Figure 7. Surface electrical resistivity test device (four-probe Wenner-Array device)

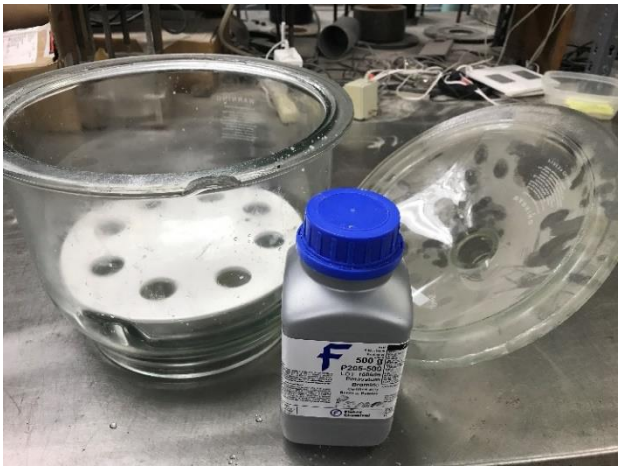

Figure 8. Preparation of a specimen for sorptivity testing

Figure 9. Measuring the CTE

Additional tests are discussed below.

Moisture Content

Interest is increasing in the assessment of the internal moisture content of concrete in the hardened state. This because the amount of water present (degree of saturation) within the pore system has a direct impact on potential freeze-thaw distress as well as other chemical-related failure mechanisms. Additionally the moisture profile across a section influences the potential for warping of a slab.

Devices to measure the relative humidity (RH) of the pore system are readily available; however, such devices may be overloaded by the placement process and the very high RH in the pores during the early life of the mixture. In addition, the property being sought is the amount of liquid water in the pores rather than the amount of vapor in the air.

Traditionally, measurement of the moisture content of a sample has involved weighing a test sample at the point of sampling after oven drying (to establish the 0% datum) and after vacuum saturation (to establish the 100% datum). Such an approach is necessarily destructive and is typically conducted in a sample several inches in size, making it impossible to obtain local information or to establish a profile in a thin element.

An alternative approach is to use capacitance-based approaches. The dielectric constant or relative permittivity of a concrete material is made up of the relative permittivity values of the material's individual constituents. As shown in Table 5, the permittivity of water is almost 20 times higher than that of other construction materials. Therefore, the dielectric constant of concrete is dependent on the volume of water in the pores. Measuring the dielectric constant is dependent on calibrating the porous system being investigated (Sakaki et al. 2011, Topp et al. 1980).

Table 5. Relative permittivity values of common materials in construction industry

Material	Relative Permittivity
Air	1
Soil mineral	3–7
Organic materials	2–5
Concrete	4–5
Ice	5
Water (20°C)	80

Figure 10 illustrates one of the most widely accepted calibration graphs suggested for soils (using equation from Topp et al. 1980). A customized calibration equation is required for both control and IC concrete mixtures.

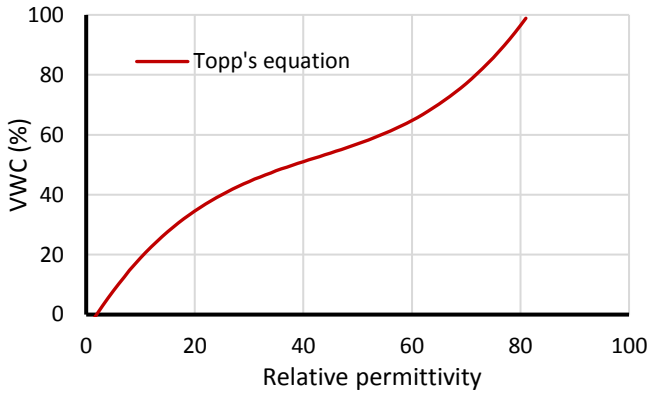

Figure 10. Practical calibration equation for different soil materials

The Decagon 5TE sensor (Figure 11) was used in this work to measure the relative permittivity of the concrete materials.

© 2015 Decagon Devices, Inc.

Figure 11. Decagon 5TE sensor for measuring relative dielectric permittivity, electrical resistivity, and temperature

The Decagon 5TE sensor is a capacitance sensor based on frequency domain technology. The sensor uses a 70 MHz frequency to minimize salinity and texture effects. The sensor also measures the temperature and electrical conductivity of the surrounding media.

Figure 12 illustrates the installation of a Decagon 5TE sensor at the top and bottom of the sidewalk slab.

Figure 12. Installation of Decagon 5TE sensors at the top and bottom layers of JPCP

The sensor should be installed horizontally with a predetermined cover of 1 in. In the laboratory study, the sensor was embedded in both directions, horizontally in a plastic pan with a 1 in. cover and vertically at the center of a 6 in. diameter cylinder. The results were almost the same, so the remaining tests were conducted using 6 in. diameter cylinders.

Pore Water Pressure in Fresh Concrete

Fresh concrete is assumed to be fully saturated at early ages, with a pore water pressure (PWP) of zero. However, as the moisture content of the mixture drops due to water consumption for hydration or from evaporation, the negative PWP increases. The variation of water content and the development of PWP in plastic concrete are illustrated in Figure 13.

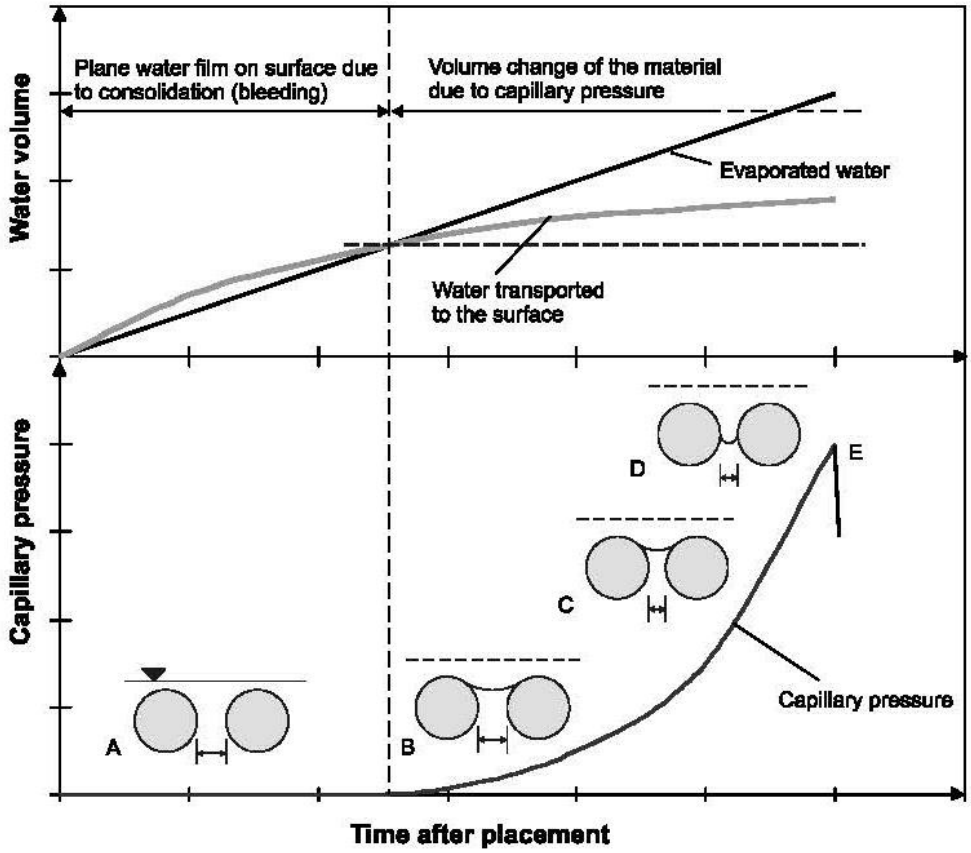

Schmidt and Slowik 2013, Copyright © 2013 ASCE, with permission from ASCE

Figure 13. Variation of water content and development of pore water pressure in early-age concrete mixtures

In Figure 13, Point A is the concrete placement time, Point B is the balance point when the rate of bleeding water is equal to the rate of missing water, and Point E is the air entry point, which is the maximum PWP the system can tolerate before cracking exposes the tip of the sensor to the atmosphere.

A high negative PWP leads to plastic shrinkage over time; if PWP exceeds a given threshold for a concrete mixture, the likelihood of plastic shrinkage cracking increases. The correlation between PWP and shrinkage strain (ε) (Wittmann 1976) highlights the need for limiting the maximum PWP and postponing the development of PWP until the concrete can carry the associated stresses. The development of PWP can be slowed by protecting the surface or by providing extra water during curing.

Figure 14 illustrates a capillary pressure sensor system (CPSS), which is used to measure PWP in plastic concrete. The hydraulic connectivity between the CPSS and the plastic concrete is provided by a small plastic syringe filled with vacuumed deionized water. The CPSS also includes a set of light, temperature, and relative humidity sensors to monitor environmental conditions at the top of the concrete surface.

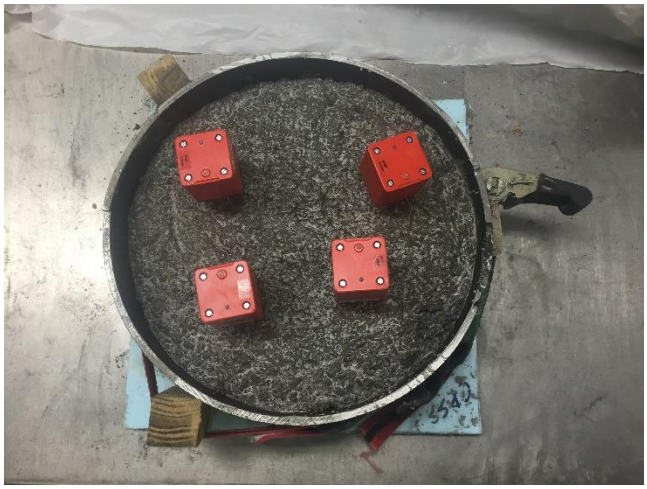

Figure 14. Capillary pressure sensor system

Portable Device for Measuring Curling and Warping of Concrete Pavements

Curling and warping of a concrete pavement are deformations that develop over time as a result of temperature and moisture gradients through the thickness of the concrete pavement. These deformations lead to increasing cyclic bending stresses at the edges of the pavement slab that can result in fatigue cracking at the corners. Figure 15 shows the upward (left) and downward (right) deformation of concrete pavement.

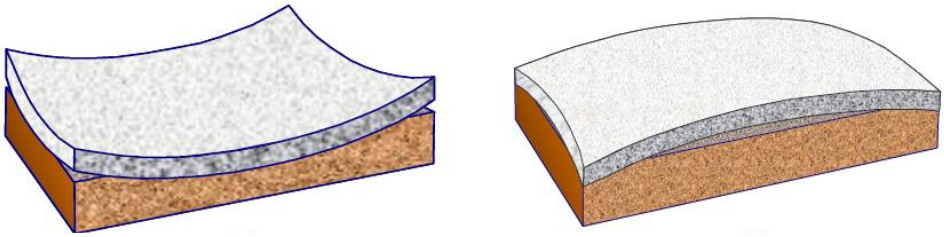

Yu et al. 2004

Figure 15. Upward (left) and downward (right) deformation of concrete pavement due to curling or warping

An inexpensive and portable device was developed at Iowa State University in 2016 to monitor curling and warping of concrete pavements over time (Ceylan et al. 2016). The benefit of this test method is that one technician can move the device and perform measurements on the site rapidly without the need for sensors to be embedded in the pavement. The test method involves installing two small steel stands at each end of the slab in the sawed joints and stretching a steel wire between them. The gap between the reference wire and the surface of the concrete slab is measured using a digital height gauge at several points along the wire. In this study, this measurement was carried out in the early morning and late evening over several months to monitor the maximum curling and warping of the pavements as a function of age and weather. Figure 16 and Figure 18 show the device and the digital height gauge, respectively.

Figure 16. Portable device for measuring deflection over time

Ceylan et al. 2016

Figure 17. Digital height gauge used for measurements

Figure 18 illustrates the measurement points on a concrete slab that are used to monitor curling and warping over time.

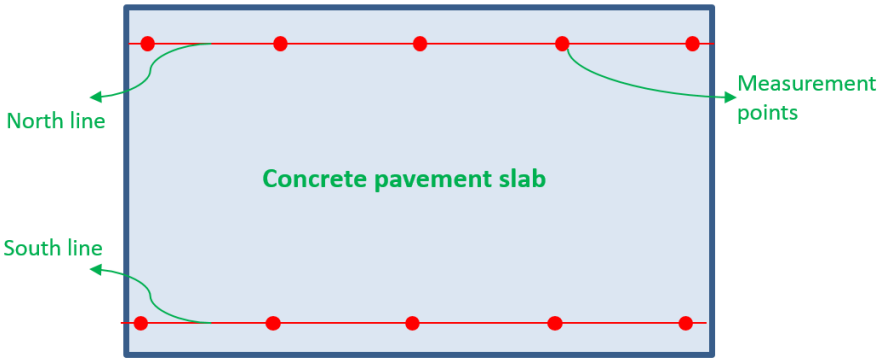

Figure 18. Ten measurement points on two lines for monitoring curling and warping on a concrete slab

As shown in Figure 18, the researchers took measurements on two parallel lines at the north and south sides of the pavement, with five measurements taken on each line.

RESULTS AND DISCUSSION

Early-Age Properties

In the laboratory study, the control concrete did not contain any water reducing admixture, but high-range water reducing agent (HRWRA) was added to the IC concrete to achieve the desired workability (2±1 in.). This shows that replacing river sand with LWFA in the mixture design may slightly decrease concrete workability. The fresh properties of the concrete mixtures, including slump, air content, and temperature, in both the laboratory and field environments are presented in Table 6 and Table 7, respectively.

Table 6. Fresh properties of concrete mixtures prepared in the laboratory

Concrete	Slump (in.)	Air Content (%)	Concrete Temperature (°F)
Control	1.75	5.0	70.5
IC	2.75	6.5	65.9

Table 7. Fresh properties of concrete mixtures sampled in the field

Concrete	Slump (in.)	Air Content (%)	Concrete Temperature (°F)
Control	4	6.1	90.0
IC	3	4.6	87.7

Local weather conditions at the time of placement (the morning of July 22, 2016) were as follows:

- Ambient temperature: 108°F
- Relative humidity: 38%
- Maximum wind speed: 9.4 mph

Figure 19 shows the results of semi-adiabatic calorimetry tests obtained for the concrete mixtures in the laboratory.

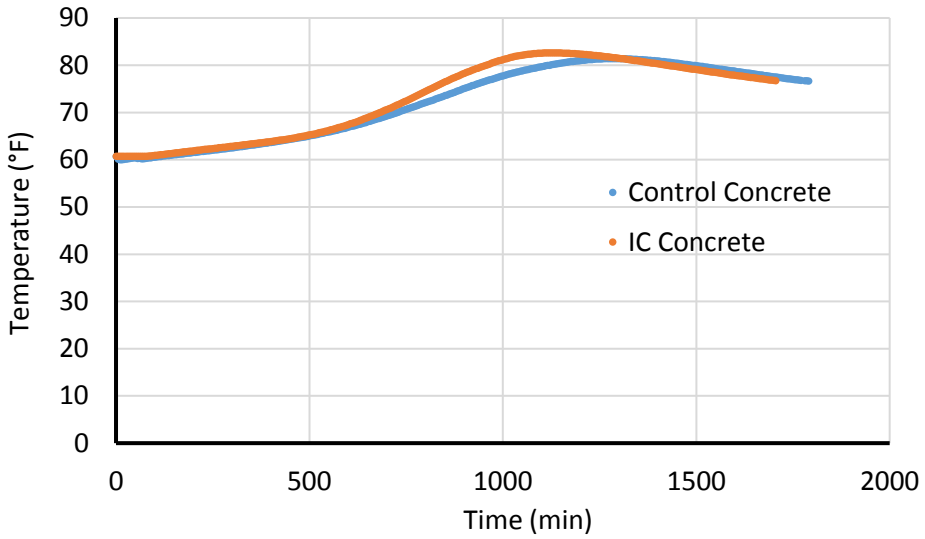

Figure 19. Semi-adiabatic calorimetry test results for laboratory mixtures

The maximum recorded temperatures and the corresponding times of peak temperature, as well as the initial setting times predicted based on calorimetry results, are summarized in Table 8. As expected, little significant difference was observed between the IC and control samples.

Table 8. Results of calorimetry test for laboratory mixtures

Concrete	Maximum Temperature (°C)	Time of Peak Temperature (min)	Initial Setting Time (min)

Control	81.4	1290	390
IC	82.6	1110	378

Figure 20 and Figure 21 show the variation in relative permittivity and electrical conductivity of mixtures investigated at early ages in the laboratory.

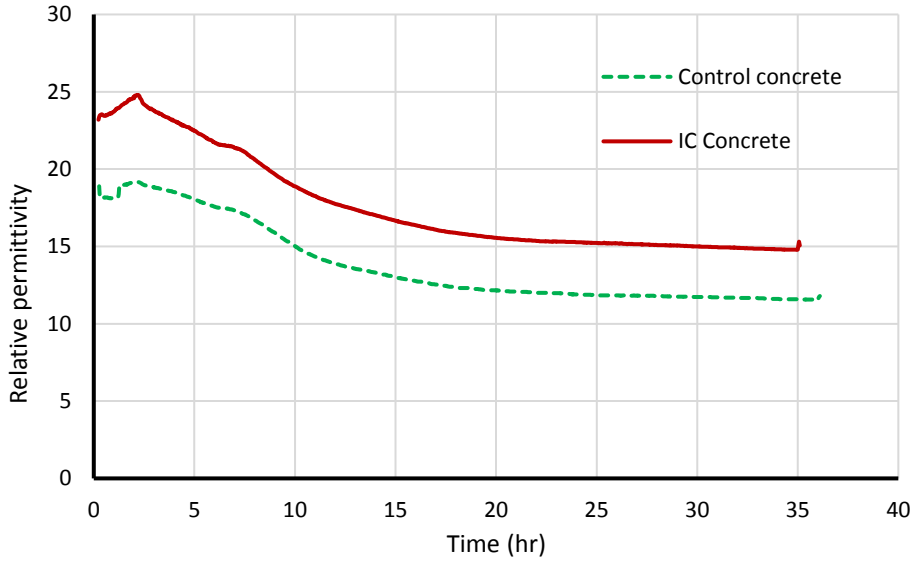

Figure 20. Variation in relative permittivity of laboratory mixtures at early ages

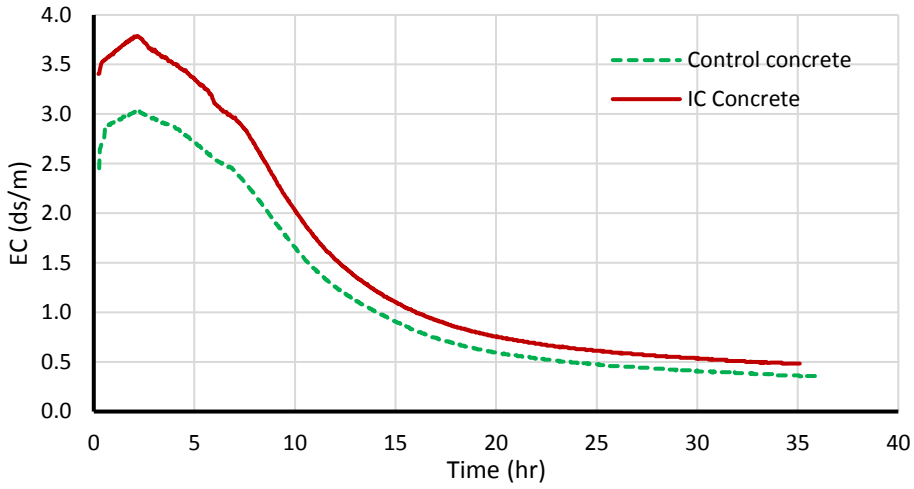

Figure 21. Variation in electrical conductivity of laboratory mixtures at early ages

Laboratory specimens were cured in closed 6 by 12 in. cylindrical specimens. IC concrete has some extra water stored in the LWA, which increases the permittivity of IC concrete mixtures compared to control concrete mixtures. As free water is removed from both systems due to hydration, the relative permittivity of both mixtures drops. According to the calorimetry test

results, cement hydration for both mixtures (Figure 20) was similar for the period monitored. Relative permittivity was in agreement, with both mixtures following almost the same trend.

The initial electrical conductivity of the IC mixture was higher at early ages, but both mixtures had almost the same conductivity after two days.

It is possible to predict both the initial and final setting time of concrete mixtures based on the variation in electrical conductivity (Li et al. 2007). The results of this analysis show that the time associated with the maximum electrical conductivity was almost the same for both mixtures (130 and 128 minutes for the control and IC mixtures, respectively) and is similar to the calorimetry test results.

Figure 22 shows the temperature variation in the control concrete in the field during the first 48 hours (measured using Decagon 5TE sensors). The first major temperature peak is due to the heat generated by hydration, while the other temperature variations follow the ambient temperature.

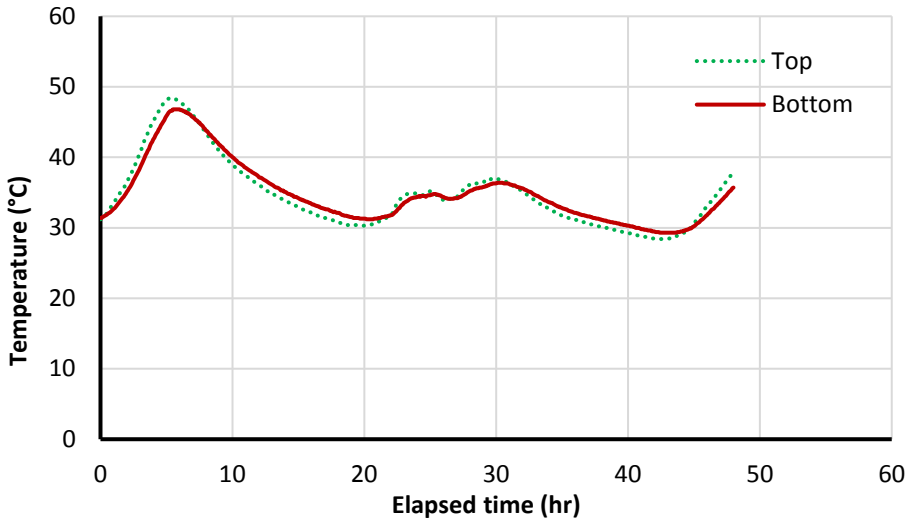

Figure 22. Temperature variation in control concrete in the field

The relative permittivity results for the control mixture are illustrated in Figure 23. Variation in the relative permittivity is mainly dependent on the moisture content of the concrete. Relative permittivity generally decreased over the first 48 hours due to moisture loss, and the decrease was initially faster at the top of the slab.

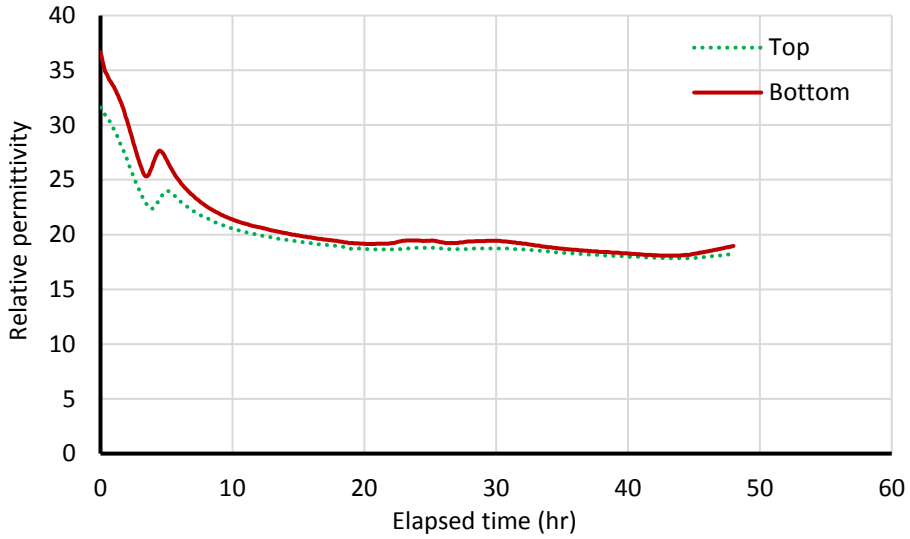

Figure 23. Relative permittivity variation in control concrete in the field

Figure 24 and Figure 25 present the variation in temperature and relative permittivity, respectively, of the IC mixture.

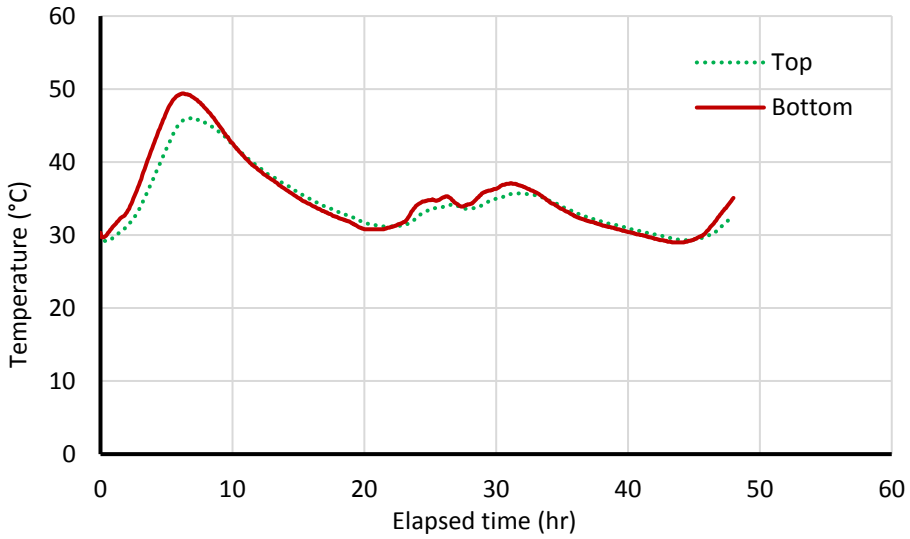

Figure 24. Temperature variation in IC concrete in the field

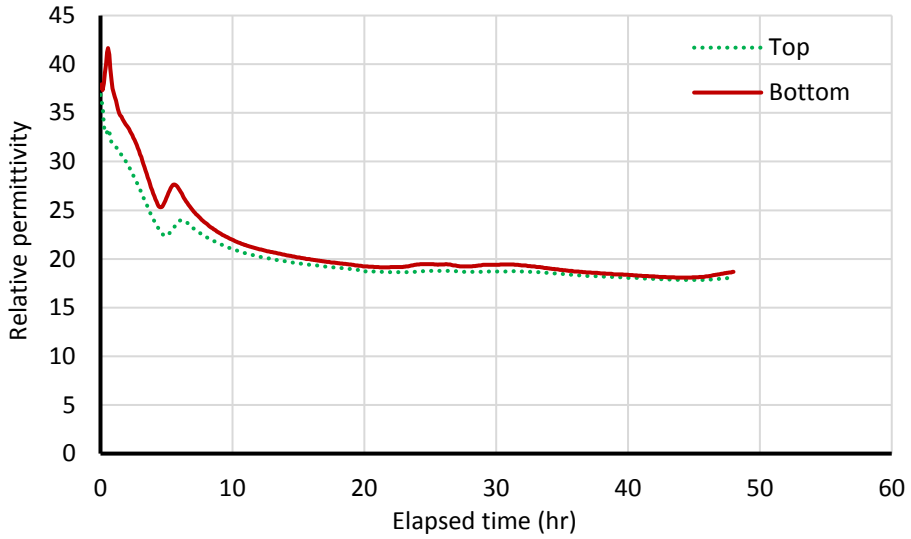

Figure 25. Relative permittivity variation in IC concrete in the field

The temperature variation in the IC concrete was similar to that in the control concrete. However, the IC concrete generally had a higher relative permittivity than the control concrete due to the stored water in the LWFA. As water was consumed due to cement hydration or evaporated due to environmental conditions in the field, the water potential increased and the LWFA released its reserved water. Both the IC and control mixtures had almost the same relative permittivity (18) at the end of the first 48-hour period.

The development of PWP in fresh concrete may contribute to plastic shrinkage strain and cracking. Figure 26 demonstrates PWP development in both control and IC concrete mixtures in the laboratory.

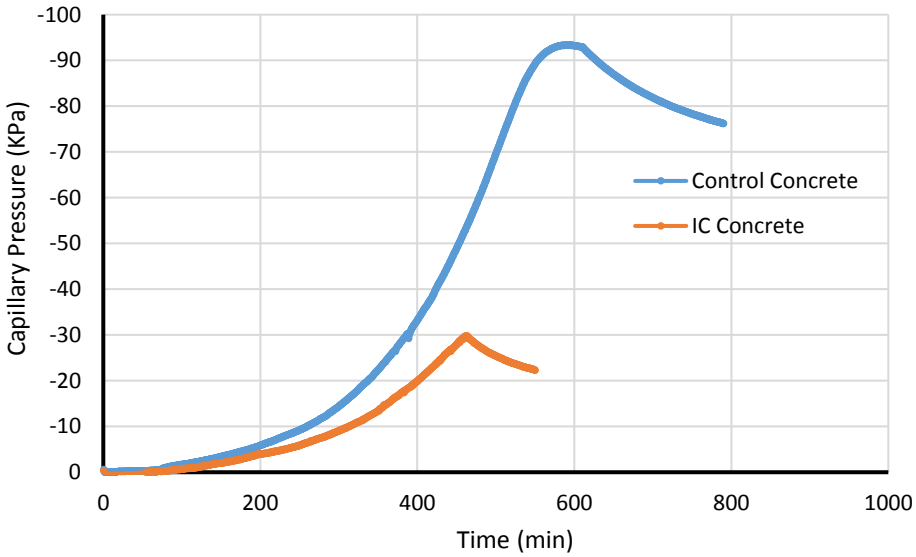

Figure 26. PWP development in fresh concrete in laboratory mixtures

Table 9 summarizes the key factors related to the development of PWP in both mixtures.

Table 9. Results of PWP development test in fresh concrete in laboratory mixtures

Concrete	Air Entry Value (KPa)	Air Entry Time (min)	Slope of Developing PWP (KPa/min)	Intercept (min)
Control	-93.41	592	-0.36	315
IC	-29.84	462.5	-0.13	243.6

The air entry value is the maximum PWP the system can tolerate. The air entry time is the time associated with the air entry value. The slope of the developing PWP is constant immediately before the air entry point.

PWP development started earlier in the control concrete and reached a value three times greater than that of the IC mixture, likely because the LWA in the IC mixture was providing water to the pores, as intended.

Hardened Properties

The mechanical properties of the control and IC concretes mixed in the laboratory and sampled in the field are reported in Table 10 and Table 11, respectively. All specimens were 4 by 8 in. cylinders demolded after the first day and then cured in a fog room until testing.

Table 10. Mechanical properties of laboratory mixtures

	Tensile Strength (psi)		Compressive Strength (psi)		MoE (ksi)	
Concrete	28-day	91-day	28-day	91-day	28-day	91-day
Control	505	683	6824	8367	6981	7047
IC	507	698	6925	8430	5461	5489

Table 11. Mechanical properties of field mixtures

	Tensile Strength (psi)		Compressive Strength (psi)		MoE (ksi)	
Concrete	28-day	91-day	28-day	91-day	28-day	91-day
Control	390	526	4785	5863	5850	5925
IC	387	529	5540	6803	4900	4925

The results indicate a 15% increase in compressive strength, while the split tensile strength was unchanged with the inclusion of the LWFA. The modulus of elasticity decreased by 15%, as expected.

It should be noted that all cylinders were subjected to standard wet curing until they were tested. Therefore, internal curing would be expected to have little influence on mechanical properties.

The trends exhibited by the control and IC mixtures were similar for both the field and laboratory mixtures, but the field mixtures were consistently weaker than the laboratory mixtures. This likely indicates differences in environment.

Laboratory and field resistivity results are shown in Figure 27 and Figure 28, respectively.

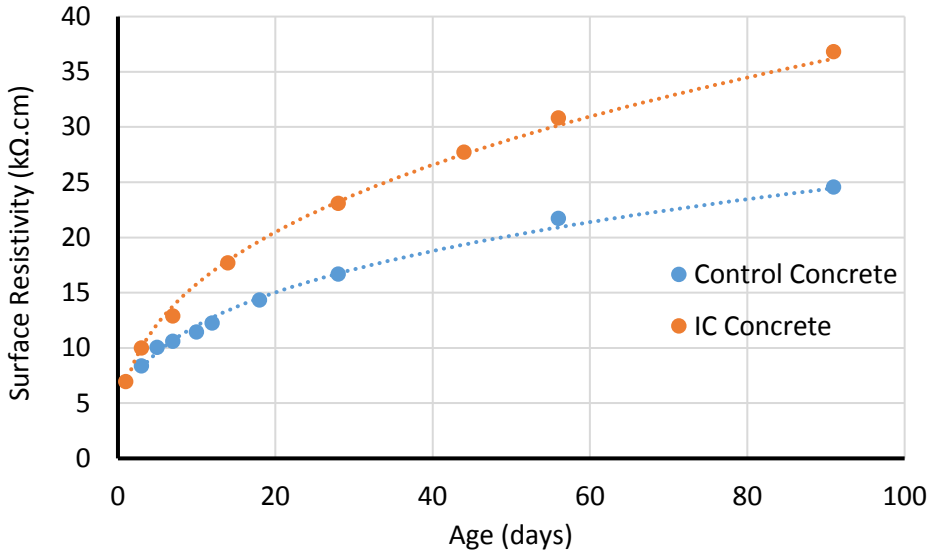

Figure 27. Surface electrical resistivity of laboratory specimens

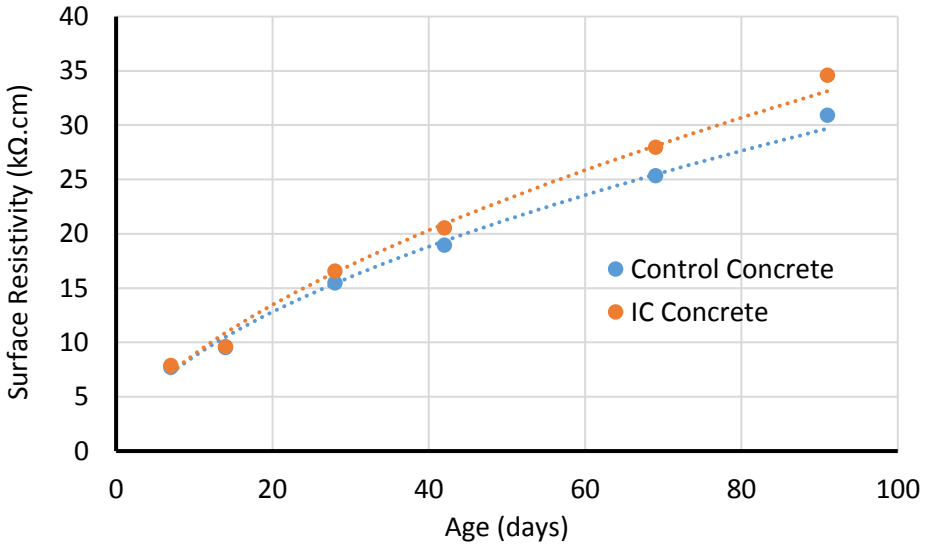

Figure 28. Surface electrical resistivity of field specimens

The results indicate that although using porous LWFA increases the total porosity of IC concrete, its permeability is lower because of the improved permeability of the paste. The effect of wetting and drying cycles at two different temperatures (50°C and 110°C) on the surface resistivity of mixtures was also investigated. The results are presented in Appendix A.

The results of water desorption, sorption, absorption, and rate of absorption (sorptivity) tests on the laboratory specimens are shown in Table 12.

Table 12. Water desorption, sorption, absorption, and rate of absorption of laboratory specimens

Concrete	Water Desorption (%)	Water Sorption (mm)	Water Absorption (%)	Rate of Absorption ($mm/s^{0.5}$)	
				Initial	Secondary
Control	4.4	4.46	3.93	12.6×10^{-4}	4.4×10^{-4}
IC	4.9	5.27	4.78	15.7×10^{-4}	4.6×10^{-4}

The tests were conducted on 4 by 8 in. cylindrical specimens at 91 days. The results show that although internal curing may improve the impermeability properties of paste (based on the results of the surface resistivity test), the water absorption properties of the IC concrete specimens are higher than those of the control concrete specimens. This is believed to be due to the effects of the porous LWA on IC concrete's absorption/desorption properties.

Figure 29 and Figure 30 show the water absorption rates of control and IC laboratory specimens, respectively, tested in accordance with ASTM C1585. Both the initial and secondary rates of water absorption increased in the IC mixtures due to the presence of porous LWFA.

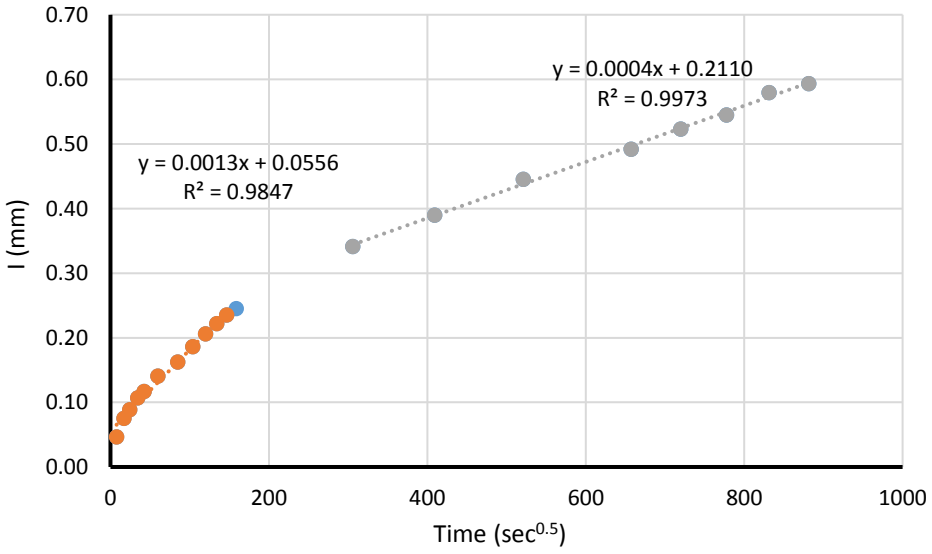

Figure 29. Sorptivity test – control concrete

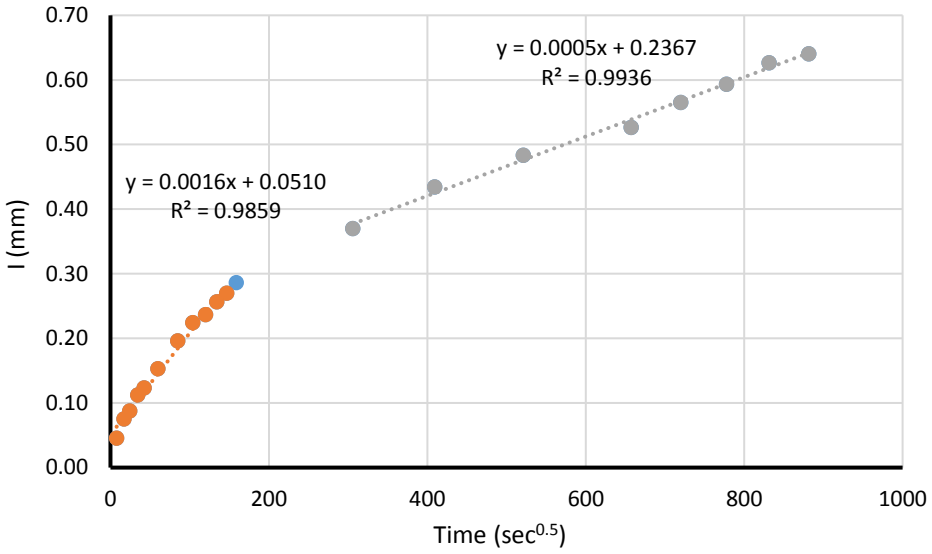

Figure 30. Sorptivity test – IC concrete

Table 13 presents the results of water desorption, sorption, and absorption tests on the field specimens.

Table 13. Water desorption, sorption, and absorption of field specimens

Concrete	Water Desorption (%)	Water Sorption (mm)	Water Absorption (%)
Control	2.23	1.79	1.83
IC	3.32	1.93	1.99

These tests were carried out on 2 in. thick disks obtained from 4 in. diameter cylinders at 28 days. The results of the tests on field specimens confirm the laboratory results and show that the incorporation of LWA increases the water absorption properties of concrete mixtures.

The CTE was determined for both the control and IC laboratory specimens at 91 days. The test was carried out on each mixture using two cylindrical specimens, each with a 4 in. diameter and 7 in. height. The average CTE values were 3.79×10^{-6} in./in./°F for the control concrete and 3.38×10^{-6} in/in/°F for the IC concrete. This difference indicates that the LWFA decreased the CTE by more than 10%.

In order to quantify the variation in the relative permittivity of hardened concrete, it is necessary to calibrate the concrete moisture content as a function of permittivity. For this purpose, a Decagon 5TE sensor was embedded at the center of a 3 by 4 by 5 in. rectangular specimen. Drying at 50°C started after seven days of wet curing. The weight and permittivity of each specimen were recorded periodically until the specimen reached constant mass. The calibration

equation for quantifying volumetric water content (VWC) based on concrete permittivity is generally nonlinear (Topp et al. 1980). However, it can be assumed to be linear over small variations in VWC, such as those found in concrete. Therefore, the equations can be evaluated as illustrated in Figure 32 for both mixtures.

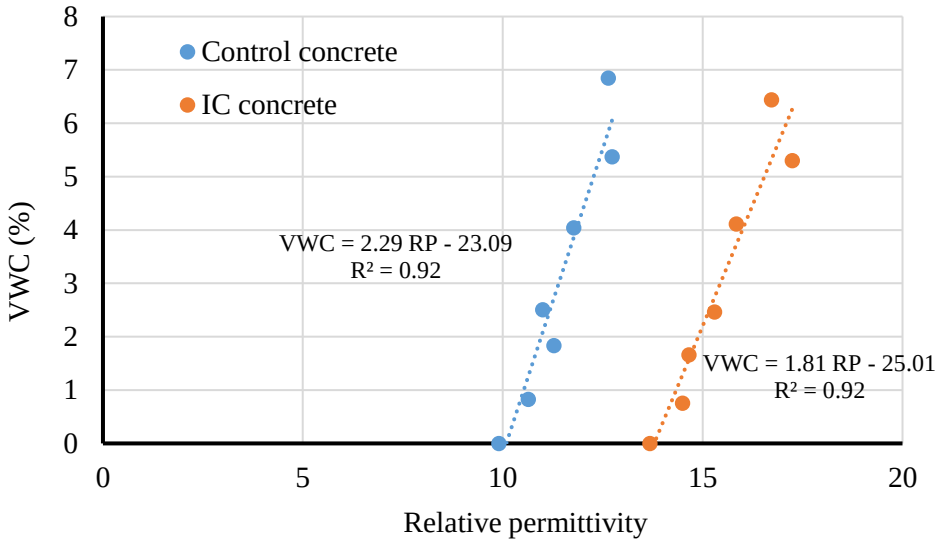

Figure 31. Customized calibration of VWC versus relative permittivity of control and IC concrete

The control concrete appears to be more conductive than the IC concrete (Figure 28), which leads to the higher energy dissipation and lower capacitance for IC concrete seen in Figure 32.

Because the pore structure and pore solution properties of cementitious materials change over time due to cement hydration, the ideal would be to develop calibrations for different ages. However, assuming that hydration slows after seven days, it can be accepted that the dielectric properties of the mixture do not vary significantly after that.

Figure 32 shows the temperature variation between the top and bottom layers of the sidewalk over time.

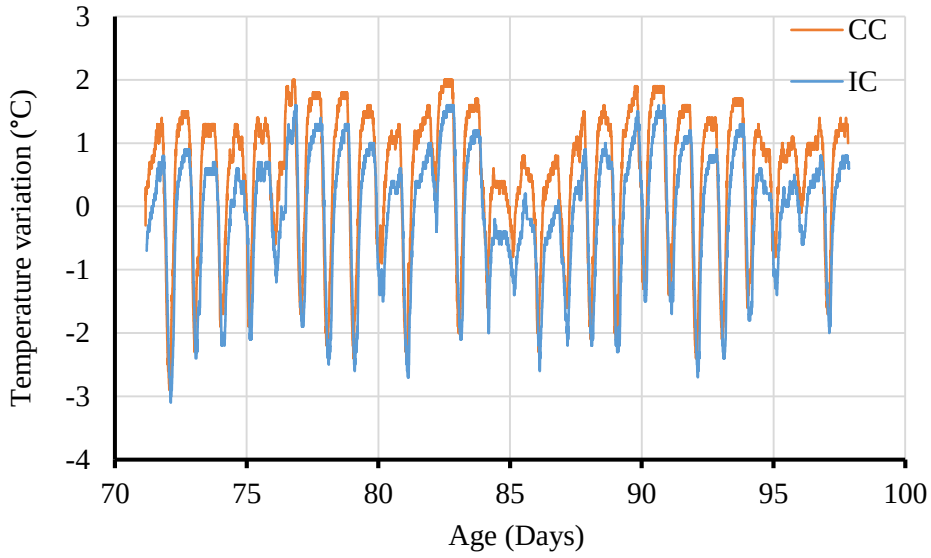

Figure 32. Temperature variation over time between top and bottom layers

The maximum recorded temperature gradient for the investigated sidewalk was less than 3°C, while the difference between the peak gradients of the IC and control concrete sections was less than half a degree. Although the resolution of the temperature sensor is 0.1°C, its accuracy is closer to ±1°C. Therefore, it can be concluded that the temperature gradients for both sections were almost the same. It is also worth noting that the thermal conductivity and specific heat capacity of the IC concrete were, respectively, lower and higher than the same properties of the control concrete (Demirboğa and Gül 2003, Uysal et al. 2004). Therefore, it seems reasonable to have obtained comparable temperature gradients for both sections.

However, Figure 33 shows that the IC concrete section exhibited a 50% lower moisture gradient through the thickness of the slab, likely because of the moisture provided by the LWFA. This lower moisture gradient has the potential to reduce potential warping in the slab.

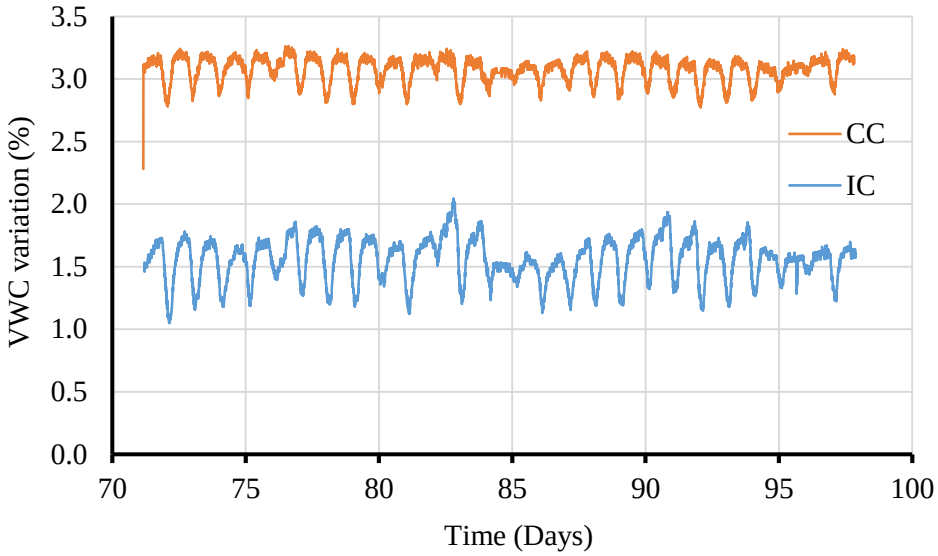

Figure 33. Variation in VWC between top and bottom layers

Curling and warping of the sidewalk were monitored using the portable device described above. Additionally, saw joints were monitored to study how they cracked in the control and IC concrete sections (Appendix B). The uncracked joint at one end of the 8 ft slab in the control section was also examined using ultrasonic shear-wave tomography to ensure there were no invisible subsurface cracks. From the results of these tests, it can be concluded that the two small 8 ft concrete slabs performed like a larger 16 ft slab.

The profile of the surface of the concrete pavements was measured in the early morning and late evening at 7 days and used as a baseline for later measurements. The measurements were repeated at the same points at 18, 76, and 96 days. The results are presented in Figure 34 through Figure 41.

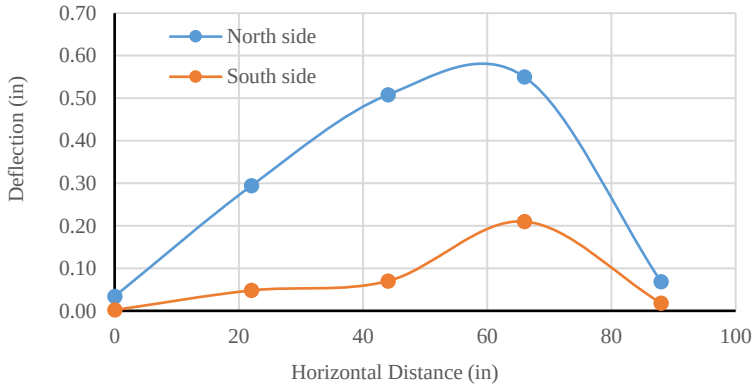

Figure 34. Built-in variation for control section, morning, 8 ft

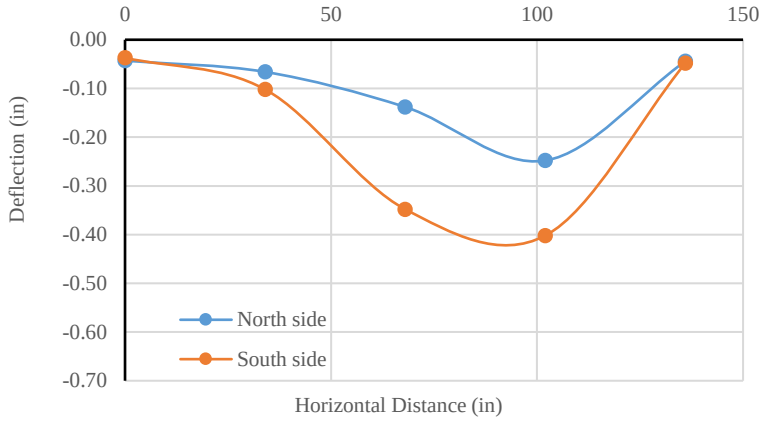

Figure 35. Built-in variation for control section, morning, 12 ft

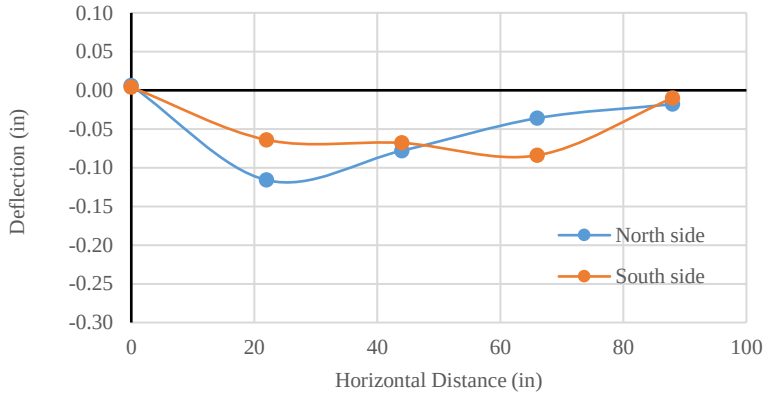

Figure 36. Built-in variation for IC section, morning, 8 ft

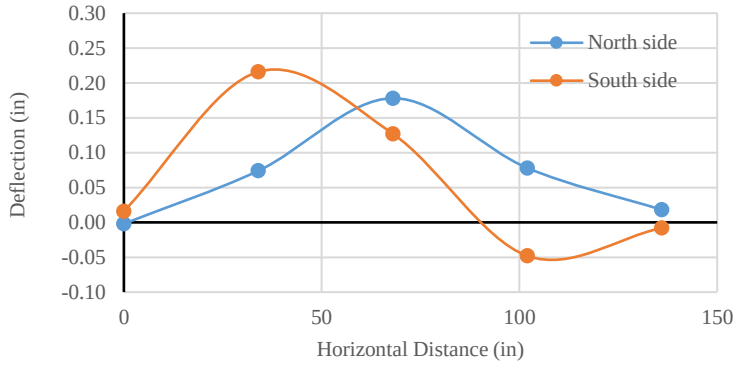

Figure 37. Built-in variation for IC section, morning, 12 ft

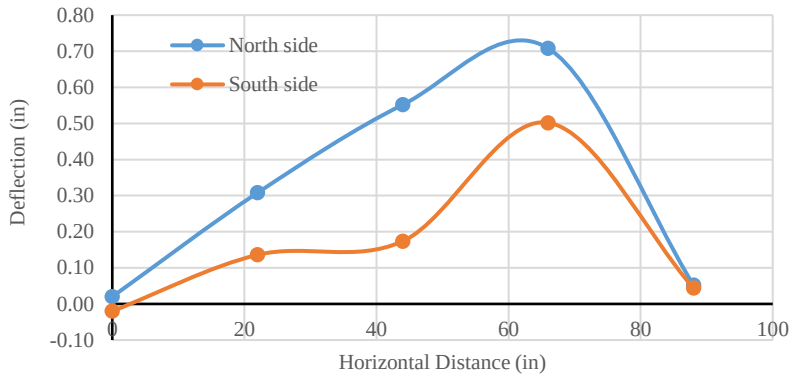

Figure 38. Built-in variation for control section, evening, 8 ft

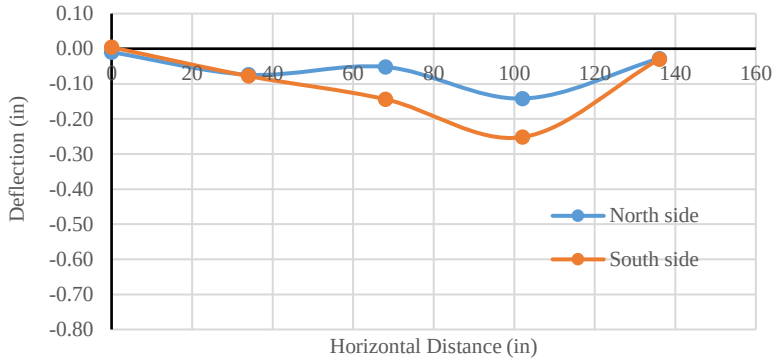

Figure 39. Built-in variation for control section, evening, 12 ft

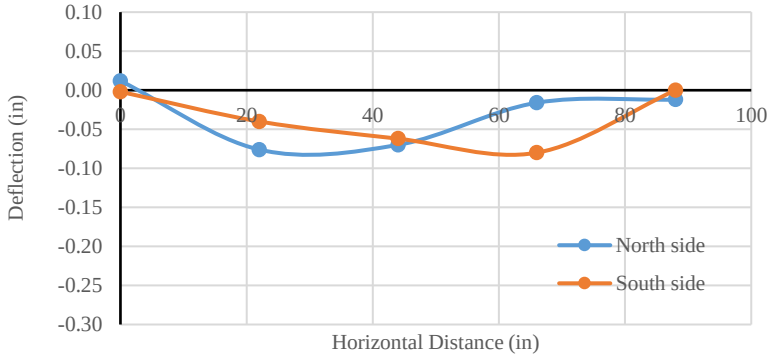

Figure 40. Built-in variation for IC section, evening, 8 ft

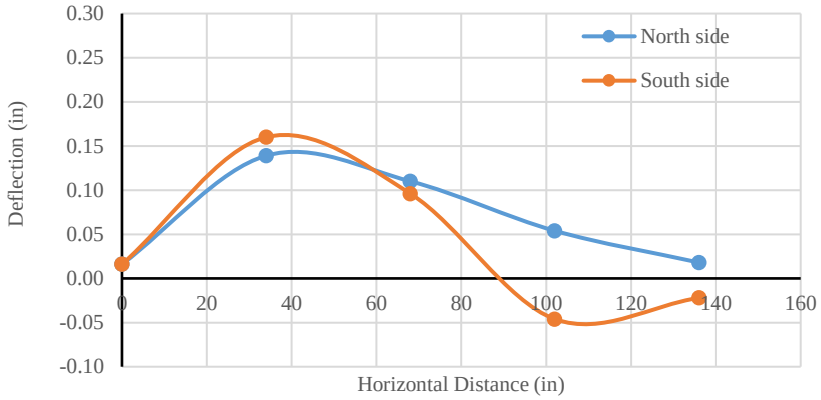

Figure 41. Built-in variation for IC section, evening, 12 ft

The maximum differential results, after compensating for the initial shape, are presented in Figure 42 through Figure 45.

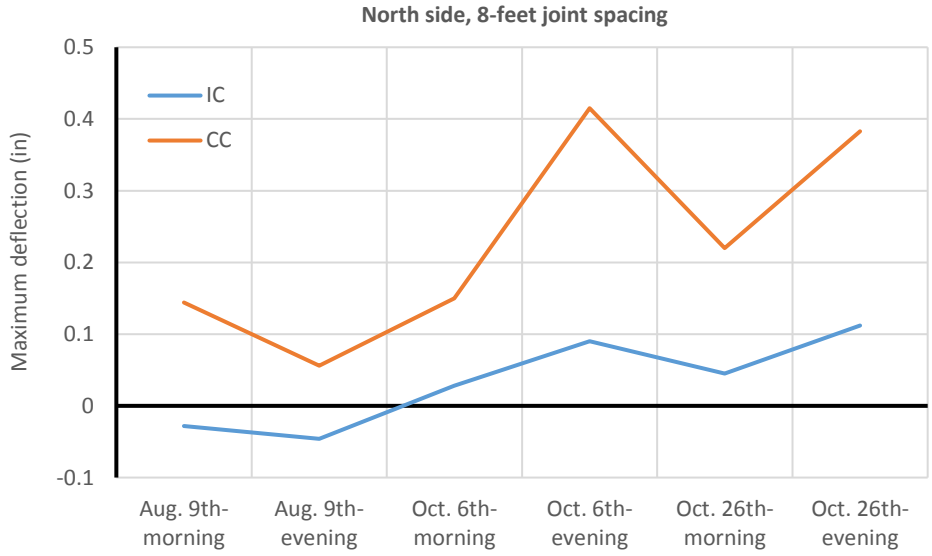

Figure 42. Curling and warping displacement at the north side of the control and IC concrete sections with 8 ft joint spacing

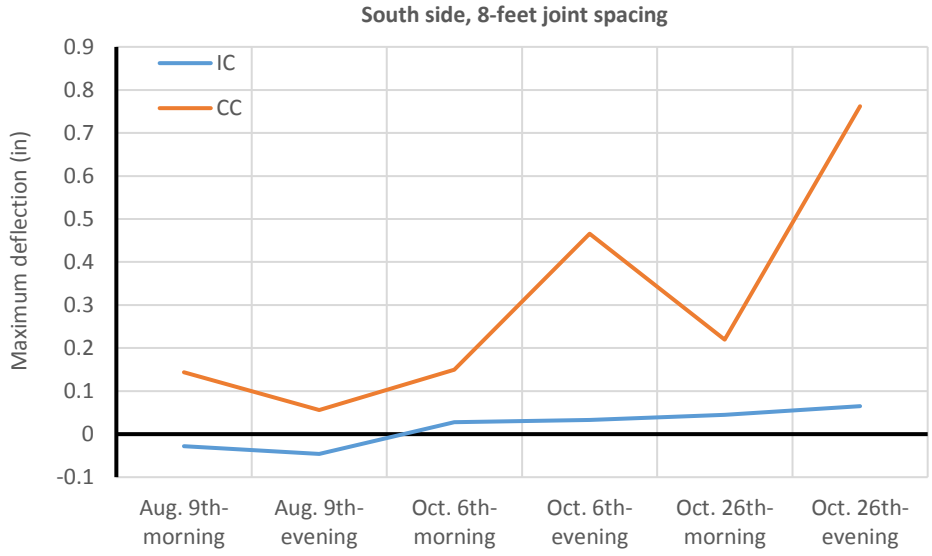

Figure 43. Curling and warping displacement at the south side of the control and IC concrete sections with 8 ft joint spacing

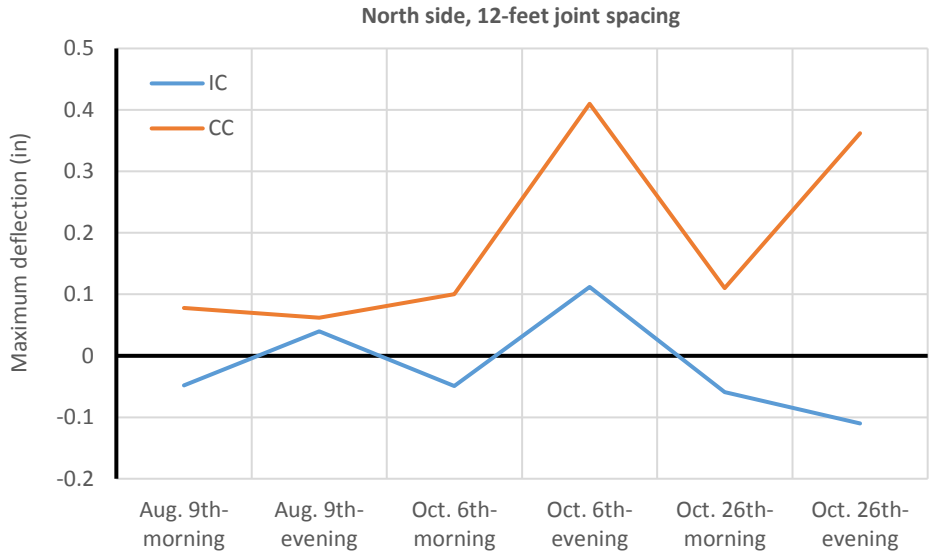

Figure 44. Curling and warping displacement at the north side of the control and IC concrete sections with 12 ft joint spacing

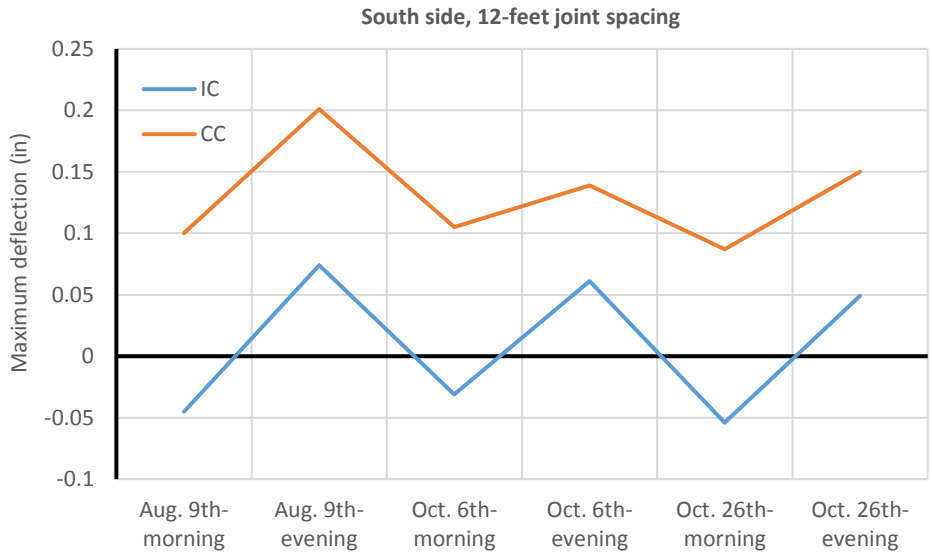

Figure 45. Curling and warping displacement at the south side of the control and IC concrete sections with 12 ft joint spacing

The results show that the IC section exhibited less curling and warping displacement for the period recorded. It may be therefore be expected that longer panels can be accommodated and/or the slabs will last longer under traffic.

Figure 46 summarizes the maximum vertical movements of the concrete pavement slabs over the measurement period.

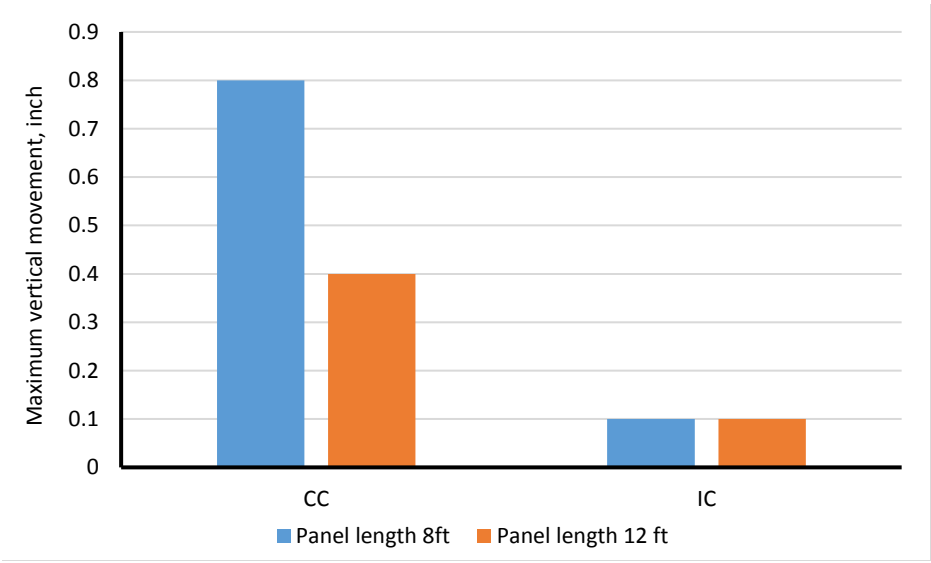

Figure 46. Summary of maximum vertical displacements

The maximum movement for the IC section is negligible compared to that of the control section. It is also worth noting that, as Appendix B shows, the joints between the 8 ft designed slabs were

not cracked. This is why the slabs performed like a larger 16 ft slab and had a maximum vertical movement almost two times higher than that of the 12 ft slabs.

CONCLUSIONS

The results of this study indicate that replacing 20% of the volume of fine aggregate with LWFA for internal curing may lead to the following results:

- The workability of the fresh concrete may slightly decrease.
- The initial setting time and heat generation are not significantly affected.
- The risk of plastic shrinkage is decreased.
- The electrical resistivity and relative permittivity are higher at early ages.
- The permeability of the cement paste is improved.
- The CTE is reduced.
- The MoE is reduced.
- Warping is reduced.

It can be concluded that although replacing a portion of the fine aggregate with LWFA for internal curing may increase the initial investment by 2.7%, the strength and durability properties of such mixtures are improved, and pavement constructed using these mixtures will last longer.

REFERENCES

ACI Committee 308 2016. *Guide to External Curing of Concrete*. American Concrete Institute, Farmington Hills, MI.

Amirkhanian, A. N. and J. R. Roesler. 2017. Unrestrained Curling in Concrete with Fine Lightweight Aggregates. *Journal of Materials in Civil Engineering*, Vol. 29, No. 9, 04017092, pp. 1–11.

Babcock, A. and P. Taylor. 2015. *Impacts of Internal Curing on Concrete Properties: Literature Review*. National Conctrete Pavement Technology (CP Tech) Center, Iowa State University, Ames, IA.

Bentz, D. P., J. M. Davis, M. A. Peltz, and K. A. Snyder. 2014. Influence of Internal Curing and Viscosity Modifiers on Resistance to Sulfate Attack. *Materials and Structures*, Vol. 47, No. 4, pp. 581–589.

Bentz, D. P. and K. A. Snyder. 1999. Protected Paste Volume in Concrete: Extension to Internal Curing Using Saturated Lightweight Fine Aggregate. *Cement and Concrete Research*, Vol. 29, No. 11, pp. 1863–1867.

Bentz, D. P. and P. E. Stutzman. 2008. Internal Curing and Microstructure of High Performance Mortars. *Internal Curing of High Performance Concretes: Laboratory and Field Experiences*, ACI SP-256, pp. 81–90.

Bentz, D. P. and W. J. Weiss. 2011. *Internal Curing: A 2010 State-of-the-Art Review*, US Department of Commerce, National Institute of Standards and Technology.

Byard, B. E. and A. K. Schindler. 2010. *Cracking Tendency of Lightweight Concrete*. Highway Research Center, Auburn, AL.

Byard, B. E., A. K. Schindler, and R. W. Barnes. 2014. Cracking Tendency of Lightweight Aggregate Bridge Deck Concrete. *Materials Journal*, Vol. 111, No. 2, pp. 179–188.

Ceylan, H., R. F. Steffes, K. Gopalakrishnan, S. Kim, S. Yang, and K. Zhuang. 2016. *Development and Evaluation of a Portable Device for Measuring Curling and Warping in Concrete Pavements*. Institute for Transportation, Midwest Transportation Center, Iowa State University, Ames, IA.

De la Varga, I., R. P. Spragg, C. Di Bella, J. Castro, D. P. Bentz, and J. Weiss. 2014. Fluid Transport in High Volume Fly Ash Mixtures with and without Internal Curing. *Cement and Concrete Composites*, Vol. 45, pp. 102–110.

Demirboğa, R., and Gül, R. 2003. The Effects of Expanded Perlite Aggregate, Silica Fume, and Fly Ash on the Thermal Conductivity of Lightweight Concrete. *Cement and Concrete Research*, Vol. 33, No. 5, pp. 723–727.

Hartman, N., T. Barrett, and J. Weiss. 2014. The Influence of Lightweight Aggregate on Internal Curing and Its Impact on Autogenous Shrinkage of High-Performance Concrete. Summer Undergraduate Research Fellowship (SURF) Symposium, Purdue University, West Lafayette, IN, August 7, 2014.

Justs, J., M. Wyrzykowski, D. Bajare, and P. Lura. 2015. Internal Curing by Superabsorbent Polymers in Ultra-High Performance Concrete. *Cement and Concrete Research*, Vol. 76, pp. 82–90.

Kim, K., T. Subgranon, M. Tia, and M. Bergin. 2016. Internally Cured Concrete for Use in Concrete Pavement Using Accelerated Pavement Testing and Finite-Element Analysis. *Journal of Materials in Civil Engineering*, Vol. 28, No. 6, 04016011, pp. 1–8.

Li, Z., L. Xiao, and X. Wei. 2007. Determination of Concrete Setting Time Using Electrical Resistivity Measurement. *Journal of Materials in Civil Engineering*, Vol. 19, No. 5, pp. 423–427.

Sakaki, T., A. Limsuwat, and T. H. Illangasekare. 2011. A Simple Method for Calibrating Dielectric Soil Moisture Sensors: Laboratory Validation in Sands. *Vadose Zone Journal*, Vol. 10, No. 2, pp. 526–531.

Schlitter, J. L., D. P. Bentz, and W. J. Weiss. 2013. Quantifying Stress Development and Remaining Stress Capacity in Restrained, Internally Cured Mortars. *Materials Journal*, Vol. 110, No. 1, pp. 3–11.

Schlitter, J., R. Henkensiefken, J. Castro, K. Raoufi, J. Weiss, and T. Nantung. 2010. *Development of Internally Cured Concrete for Increased Service Life*. Joint Transportation Research Program, Purdue University, West Lafayette, IN.

Schmidt, M. and V. Slowik. 2013. Capillary Pressure Controlled Concrete Curing in Pavement Construction. ASCE Conference Proceedings, *Airfield and Highway Pavement 2013: Sustainable and Efficient Pavements*, pp. 295–306.

Shen, D., H. Shi, X. Tang, Y. Ji, and G. Jiang. 2016. Effect of Internal Curing with Super Absorbent Polymers on Residual Stress Development and Stress Relaxation in Restrained Concrete Ring Specimens. *Construction and Building Materials*, Vol. 120, pp. 309–320.

Shen, D., T. Wang, Y. Chen, M. Wang, and G. Jiang. 2015. Effect of Internal Curing with Super Absorbent Polymers on the Relative Humidity of Early-Age Concrete. *Construction and Building Materials*, Vol. 99, pp. 246–253.

Sun, X., B. Zhang, Q. Dai, and X. Yu. 2015. Investigation of Internal Curing Effects on Microstructure and Permeability of Interface Transition Zones in Cement Mortar with SEM Imaging, Transport Simulation, and Hydration Modeling Techniques. *Construction and Building Materials*, Vol. 76, pp. 366–379.

Topp, G. C., J. Davis, and A. P. Annan. 1980. Electromagnetic Determination of Soil Water Content: Measurements in Coaxial Transmission Lines. *Water Resources Research*, Vol. 16, No. 3, pp. 574–582.

Uysal, H., R. Demirboğa, R. Şahin, and R. Gül. 2004. The Effects of Different Cement Dosages, Slumps, and Pumice Aggregate Ratios on the Thermal Conductivity and Density of Concrete. *Cement and Concrete Research*, Vol. 34, No. 5, pp. 845–848.

Wittmann, F. 1976. On the Action of Capillary Pressure in Fresh Concrete. *Cement and Concrete Research*, Vol. 6, No. 1, pp. 49–56.

Wyrzykowski, M. and P. Lura. 2015. Reduction of Autogenous Shrinkage in OPC and BFSC Pastes with Internal Curing. *Proceedings of the XIII Conference on Durability of Building Materials and Components*, pp. 999-1005.

Yu, H. T., L. Khazanovich, and M. I. Darter. 2004. Consideration of JPCP Curling and Warping in the 2002 Design Guide. 83rd Annual Meeting of the Transportation Research Board, Washington, DC, January 2004. Available at: www.researchgate.net/profile/Thomas_Yu2/publication/275642592_Consideration_of_JPCP_Curling_and_Warping_in_the_2002_Design_Guide/links/554145150cf2718618dc9dd0/Consideration-of-JPCP-Curling-and-Warping-in-the-2002-Design-Guide.pdf.

APPENDIX A: CYCLIC WETTING AND DRYING REGIME

Environmental cyclic loading (like moisture or temperature variation) can affect the transport properties of concrete by making microcracks in the pore structure of concrete. In this study, two control and two IC concrete specimens (4 by 8 in. cylinders) were investigated under wetting and drying cycles at the age of 91 days. Specimens were fully immersed in lime-saturated water for the wetting cycles and dried in ovens at two different temperatures, 50°C and 110°C, to represent normal and extreme temperature loading, respectively. Each wetting or drying cycle was stopped when the specimen reached a constant weight. The surface resistivity of the saturated specimens was then measured at the laboratory's room temperature to indicate the permeability of the concrete specimen.

As demonstrated in Figure 48, drying the control specimens in an oven at 50°C increased resistivity, as expected. The resistivity of the IC concrete increased by a higher amount, likely due to improved hydration.

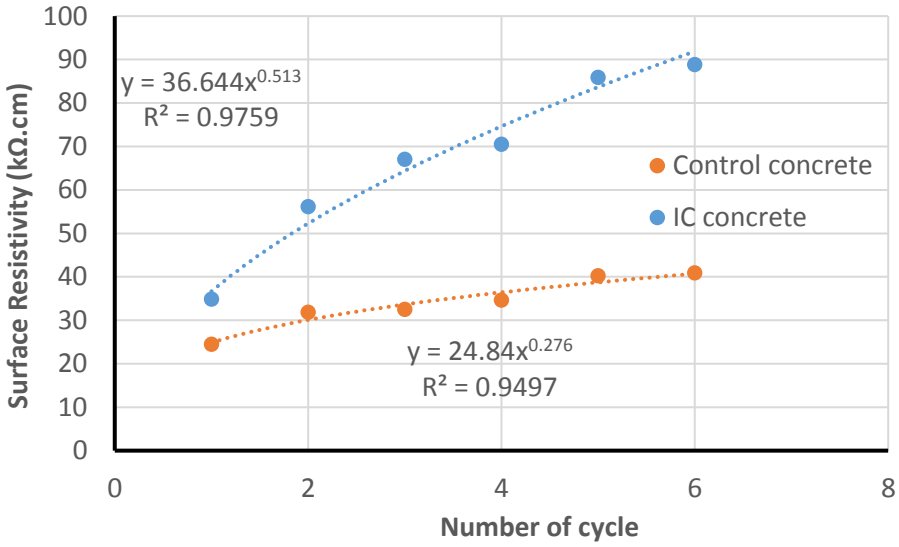

Figure 47. Cyclic wetting and drying regime at 50°C

In contrast, drying the specimens at 110°C significantly adversely affected concrete permeability (Figure 49), likely by propagating microcracks in the pore structure. The detrimental effects of temperature loading were significant in the first cycles.

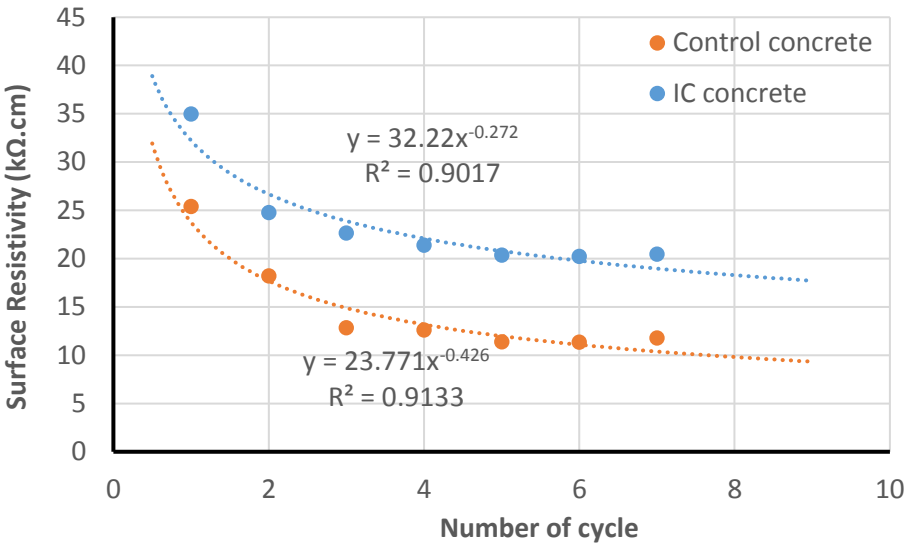

Figure 48. Cyclic wetting and drying regime at 110°C

APPENDIX B: MONITORING JOINT CRACKING OF CONTROL AND IC SECTIONS

The schematic plan of the joints in the control section is illustrated in Figure 49.

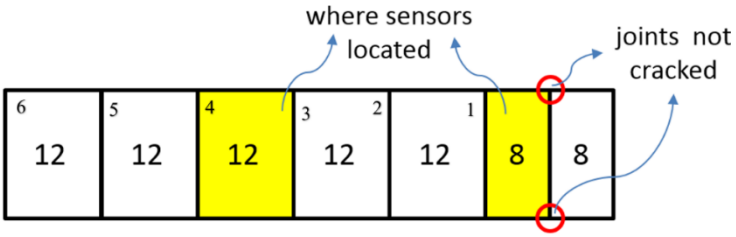

Figure 49. Schematic plan of joints in the control section

As illustrated, only two of the joints located at the very beginning of the pavement were not cracked (monitored in July 2017). Joints 1 through 6, which were all cracked, are shown with scales in Figure 50 through Figure 55.

Figure 50. Joint 1 in the control section

Figure 51. Joint 2 in the control section

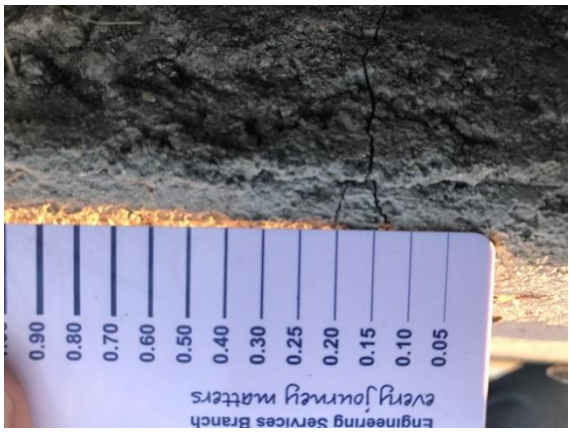

Figure 52. Joint number 3 in the control section

Figure 53. Joint 4 in the control section

Figure 54. Joint 5 in the control section

Figure 55. Joint 6 in the control section

In addition, the uncracked joint between the 8 ft slabs in the control section was investigated using ultrasonic shear-wave tomography to determine whether invisible cracks were present. The device for performing ultrasonic shear-wave tomography, MIRA, contains 40 dry point contact (DPC) transducers in total, which can send and receive low-frequency (55 kHz) shear-wave ultrasonic pulses. The transducers are placed in 10 channels (each channel has four transducers) and are able to conduct 45 transmitting and receiving pair measurements during each test. The test was repeated 10 times, and the average results are presented in Figure 56.

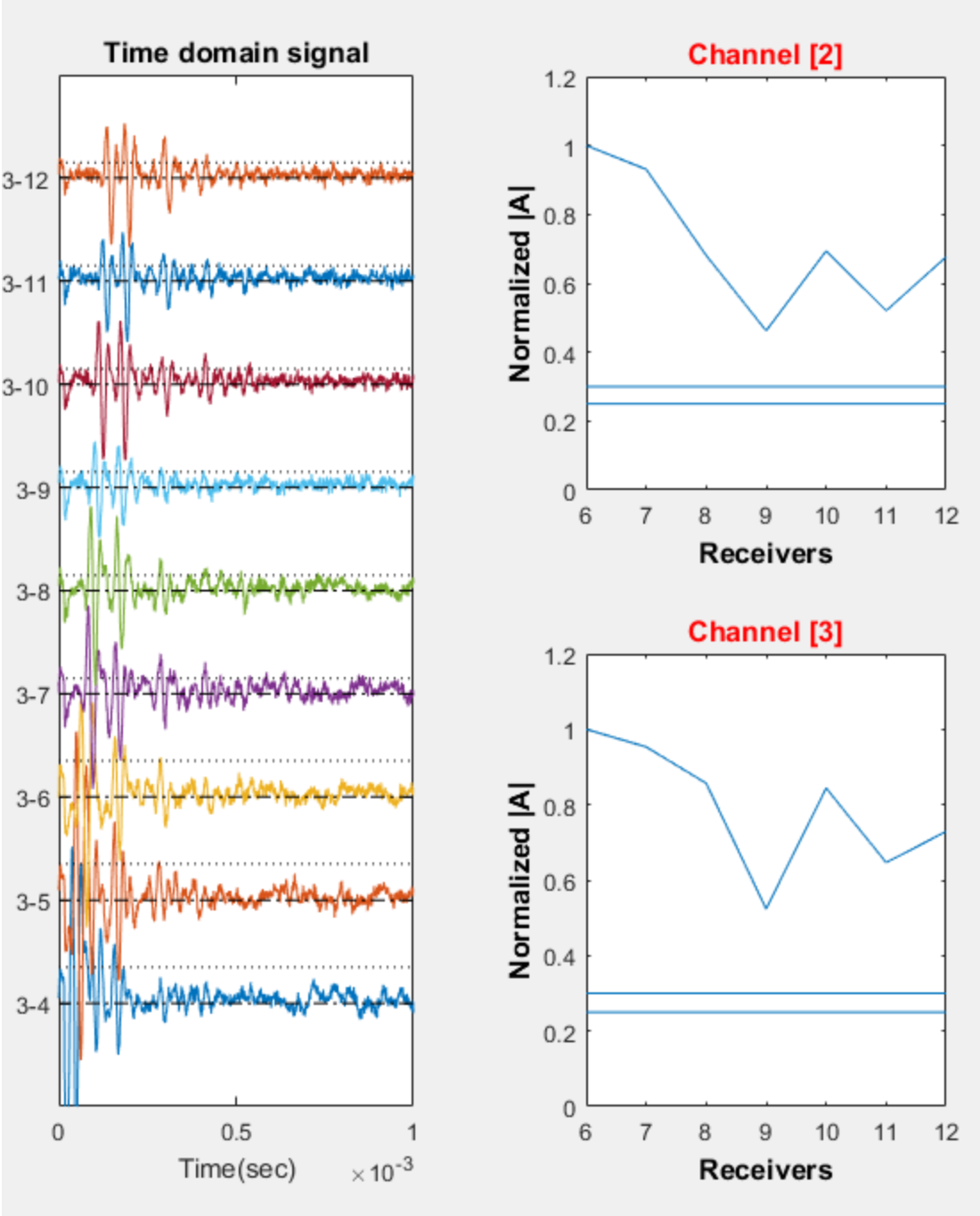

Figure 56. Results of ultrasonic shear-wave tomography for cracked joints diagnostics

The results showed that no invisible subsurface cracks were present in the joint, and the two 8 ft slabs performed like one large 16 ft slab in practice.

A schematic plan of the joints in the IC section is illustrated in Figure 57.

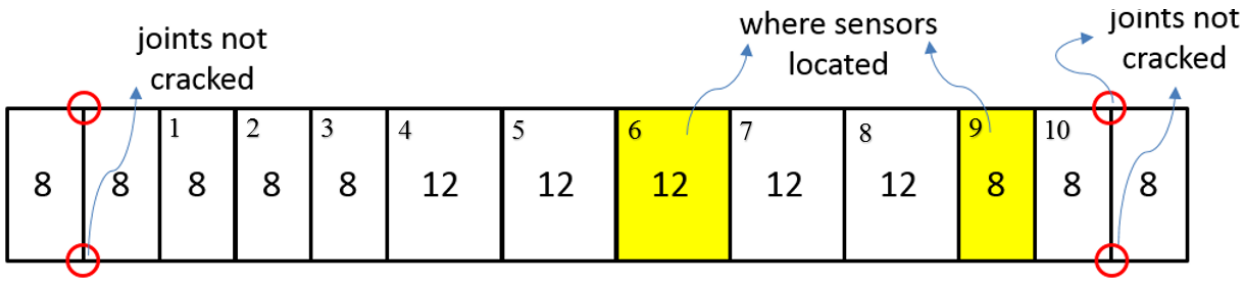

Figure 57. Schematic plan of joints in the IC section

As presented, only two sets of joints, one at each end of the pavement, were not cracked. Joints 1 through 10 in the IC section, which were all cracked, are shown with scales in Figure 58 through 67.

Figure 58. Joint 1 in the IC section

Figure 59. Joint 2 in the IC section

Figure 60. Joint 3 in the IC section

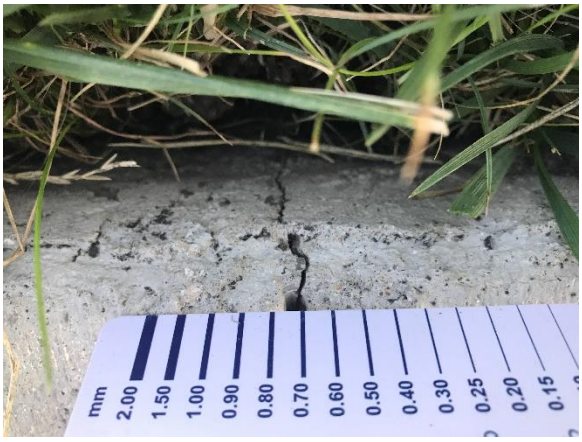

Figure 61. Joint 4 in the IC section

Figure 62. Joint 5 in the IC section

Figure 63. Joint 6 in the IC section

Figure 64. Joint 7 in the IC section

Figure 65. Joint 8 in the IC section

Figure 66. Joint 9 in the IC section

Figure 67. Joint 10 in the IC section

THE INSTITUTE FOR TRANSPORTATION IS THE FOCAL POINT FOR TRANSPORTATION AT IOWA STATE UNIVERSITY.

InTrans centers and programs perform transportation research and provide technology transfer services for government agencies and private companies;

InTrans manages its own education program for transportation students and provides K-12 resources; and

InTrans conducts local, regional, and national transportation services and continuing education programs.

IOWA STATE UNIVERSITY

Visit www.InTrans.iastate.edu for color pdfs of this and other research reports.